이학석사학위논문

이리듐 기반 인광/전기화학발광 글루타티온 센서

Iridium(III) Complex-based Phosphorescent and Electrochemiluminescent Dual Sensor for Selective Detection of Glutathione (GSH)

2021 년 2 월

서울대학교 대학원

화학부 유기화학 전공

노 현 승

이리듐 기반 인광/전기화학발광 글루타티온 센서

Iridium(III) Complex-based Phosphorescent and Electrochemiluminescent Dual Sensor for Selective Detection of Glutathione (GSH)

지도교수 홍 종 인

이 논문을 이학석사학위 논문으로 제출함.

2021년 2월

서울대학교 대학원 화학부

유기화학전공

노 현 승

노현승 의 이학 석사 학위논문을 인준함.

2021년 2월

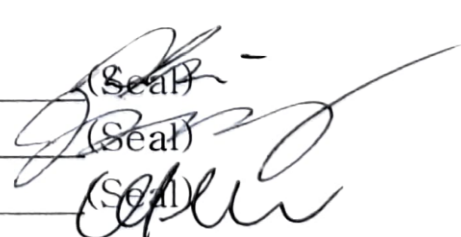|		
Chair	민 달 희	(Seal)
Vice Chair	홍 종 인	(Seal)
Examiner	이 현 우	(Seal)

Abstract

Iridium(III) Complex-based Phosphorescent and Electrochemiluminescent Dual Sensor for Selective Detection of Glutathione (GSH)

Hyun Seung NO

Major in Organic Chemistry

Department of Chemistry

Graduate School

Seoul National University

Glutathione (GSH) is a tripeptide composed of three amino acids, cysteine, glutamic acid and glycine. It is the most abundant biological thiol and used as a reducing agent in human cells. Glutathione deficiency is related to oxidative stress which may lead to progression of cancer. Therefore, a selective detection method for GSH is highly required.

Here, we report iridium complex-based photoluminescent and electrochemiluminescent sensors (1-3) for the selective detection of GSH. Sensors 1-3 consist of a 1,10-phenanthroline-5,6-dione (pdo) ancillary ligand as a common reaction site for GSH and 2-phenylpyridine, 1-phenylisoquinoline, and 2-phenylquinoline as main ligands, respectively. The three sensors were prepared to compare the effect of main ligands on the sensitivity and selectivity

of GSH detection. All three sensors showed selective turn-on photoluminescence (PL) and turn-off electrochemiluminescence (ECL) response toward GSH among biological thiols. In particular, sensor **1** with a 2-phenylpyridine main ligand showed the most selective and sensitive sensing behavior toward GSH in both PL and ECL. The pdo moiety of **1-3** is reduced to 1,10-phenanthroline-5,6-diol of **1-GSH** (or **2-GSH, 3-GSH**) upon reaction with GSH. The formation of diol in **1-GSH** was demonstrated by the FT-IR, NMR, Mass spectrometry and UV-Vis analyses.

The PL turn-on and ECL turn-off sensing mechanisms of sensor **1** were investigated by density functional theory (DFT) calculations and electrochemical studies. DFT calculations revealed that the electron density of the lowest unoccupied molecular orbital is mainly localized on the di-carbonyl moiety of **1**, providing non-radiative pathways, which is cut off by the diol moiety of **1-GSH**. The HOMO and LUMO energy levels obtained by DFT calculations were also confirmed by CV measurements. The cyclic voltammetry of a mixture of **1** and GSH showed that the phenolic radical species produced at an anodic potential suppresses the ECL process. Sensor **1** was successfully applied to the determination of GSH concentrations in human serum samples by PL and ECL methods.

Keyword: Glutathione (GSH), Iridium Complex, Small Molecular Sensor, Photoluminescence (PL), Electrochemiluminescence (ECL), Cyclic Voltammetry.
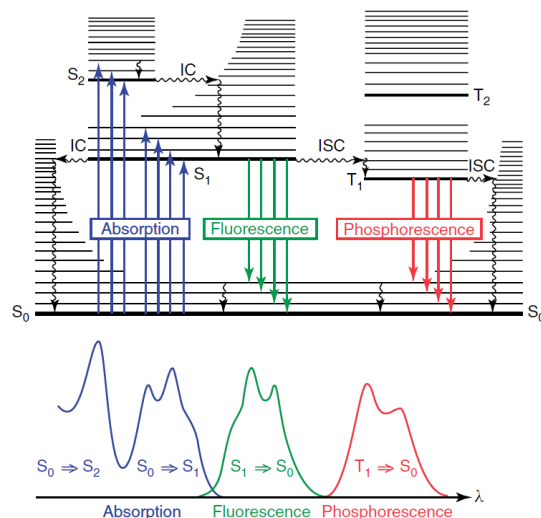
Student Number: 2019-26006

Contents

Chapter 1. Background

1.1. Design Principle of Photoluminescent Sensor


Figure 1. Jablonski diagram and relative position of the spectra. (Reproduced with permission from Valeur (2002). Copyright Wiley)

Fundamentals of Photoluminescence

Photoluminescence is light emission caused by the absorption of photons after the irradiation of a substance. The electrons in ground state were excited to a higher energy level followed by various relaxation or transition process including internal conversion (IC), fluorescence, intersystem crossing (ISC), phosphorescence, and so on. The electronic states of a molecules and the transition between these states could be well depicted by Jablonski diagram (Figure 1)[1].

Photoluminescence is one of the most powerful tools for the analysis of many analytes due to their non-invasiveness, high sensitivity and selectivity, rapid response and operational simplicity. As a result, commercially available instrument using PL provides superb manipulability, and lower detection limit which is highly required for the development of biological and environmental analysis[2].

## 1.1.1 Design Strategies of optical signaling system
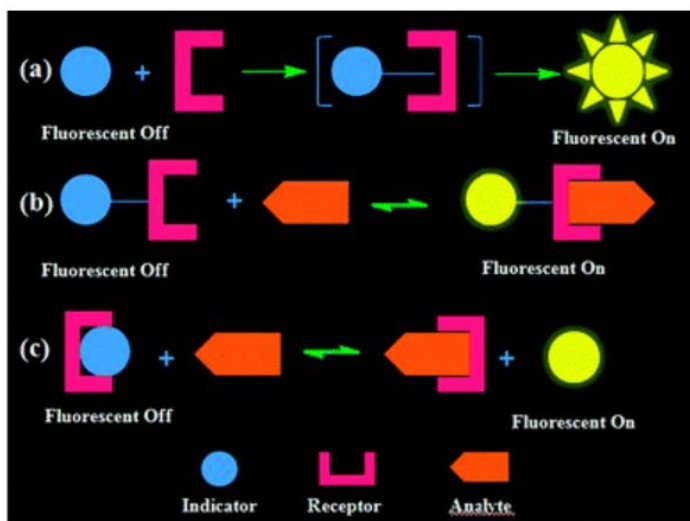
Figure 2. The three main approaches for sensing anions: (a) chemodosimeter; (b) chemosensor bearing a signaling subunit as well as a binding site; (c) displacement approach.

A photoluminescent chemosensor is a small molecular system capable of interacting with specific target molecules to detect changes in luminescence caused by the change in physicochemical properties (Figure 2)[3]. There are several design methods to construct chemosensor. The first thing is using specific chemical reactions after binding with target analyte. (Figure 2a). The second thing requires the covalent binding sites that can induce a change of signal to the chemosensors (Figure 2b). The third one uses displacement approach that the presence of target molecule liberates the indicator and recovers the intrinsic luminescence of fluorophore (Figure 2c).

The intramolecular interactions (e. g. photo-induced electron transfer (PeT), Förster resonance energy (FRET), excited-state intramolecular proton transfer (ESIPT) and aggregation-induced emission (AIE)) between fluorophore and receptor is essential for design of chemosensor.

## 1.1.2 Photo-induced electron transfer (PeT)
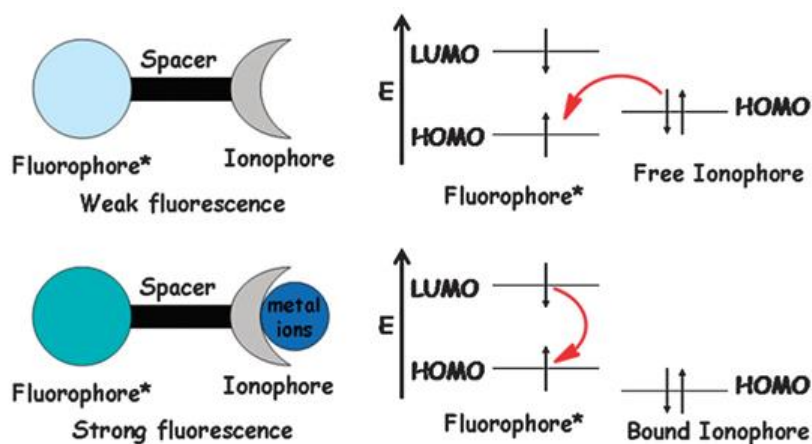
Figure 3. PeT fluorescent probes for metal cations and their turn-on sensing mechanism.

Photo-induced electron transfer (PeT) is a process that an excited electron is transferred from donor to acceptor. Most PeT chemosensors consist of three part; fluorophore, spacer (or linker) and ionophore (Figure 3)[2]. Before binding with target analyte, the ionophore HOMO (highest occupied molecular orbital) situate between the fluorophore HOMO and LUMO (lowest occupied molecular orbital) energy level. After the photo-excitation, the electron existing in fluorophore HOMO excite to the LUMO, then, the electron of the ionophore HOMO could be transferred to the HOMO of the excited fluorophore. Subsequently, the excited electron existing in fluorophore LUMO transferred to the ionophore HOMO non-radiatively, resulting in non-emissive transition of fluorophore.

After binding with target analyte, however, fluorophore retrieve the radiative transition by inhibition of electron transfer due to the decreased ionophore HOMO energy level than fluorophore HOMO. PeT is the most popularly used mechanism for design of chemosensors.

## 1.1.3 Forster resonance energy transfer (FRET)
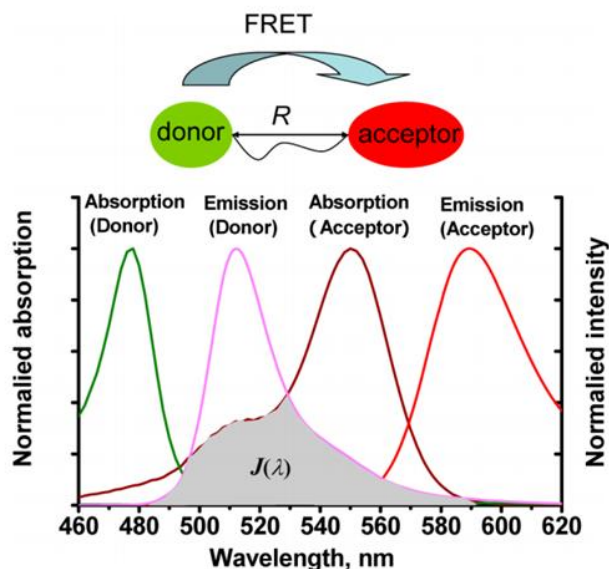
Figure 4. Schematic of the FRET process.

Foster (or Fluorescence) resonance energy transfer (FRET) is a distance-dependent interaction between the electronic excited states of two fluorophore (donor and acceptor), After photo-excitation of donor fluorophore, excitation is transferred to an acceptor without emission of a photon (Figure 4)[4]. There are some demanding conditions for designing effiecint FRET system.

(1) The absorption spectrum of the donor and acceptor should be separated to ensure independent excitation.

(2) The emission spectrums of the donor and acceptor should be resolved from that of the acceptor, to minimize the effect of each other's measurement.

(3) High photoluminescence quantum yield is required for both fluorophores to obtain marked difference before and after the reaction with target analyte.

(4) As close contact between fluorophores cause static quenching, appropriate linkers should be inserted between the donor and acceptor.

## 1.1.4 Excited-state intramolecular proton transfer (ESIPT)
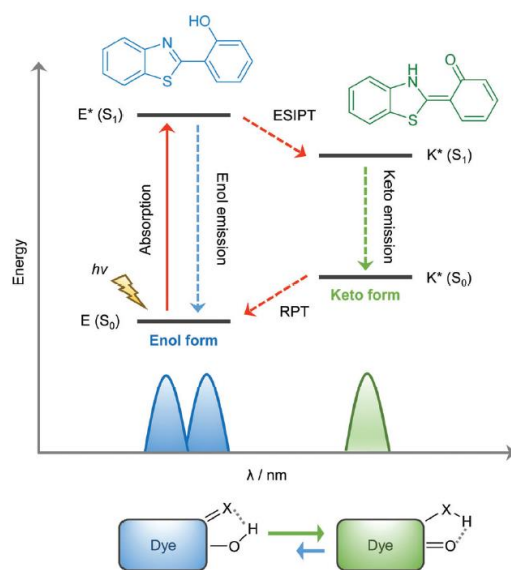
Figure 5. Diagrammatic description of the ESIPT process.

Excited-state intramolecular proton transfer (ESIPT) is a four-level photochemical process. Most of ESIPT fluorophores have an enol (E) form in ground state. The electron distribution can be redistributed after photoexcitation, allowing more electrons to the alcohol group and less electrons to the alkene group. As a result, the excited state proton of alcohol is transferred to alkene group and enol excited state converts to its excited keto form (K^*), which is called phototautomerization. After de-excitation to its electronic ground state (K), a reverse proton transfer takes place to produce the original enol form (Figure 5)[5].

ESIPT fluorophore shows dual-emission spectra, because of different emission wavelength of excited state enol (E^*) and keto (K^*) form and this is utilized in ratiometric sensor. Ratiometric probes are very useful for fluorescence detection of biologically and environmentally important species, as it provides direct information about the concentration of the target analyte without the need for calibration.

1.1.5 Aggregation Induced Emission (AIE)

Concentration quenching is a widely known process in which luminescence is decreased at high concentration of fluorophore. most organic fluorophores have low solubility in water, thus, they form the aggregates in aqueous media. For example, the perylene rings form aggregate in aqueous solution and may experience strong pi–pi stacking interactions (Figure 6a)[6], resulting in lower photoluminescence by the formation of excimers. This quenching effect caused by aggregation is referred as "Aggregation caused quenching" (ACQ). In 2001, B. Z. Tang et al. discovered a unique fluorescent process in which aggregation increase the luminescence, rather than decrease as in the ACQ systems. they termed the process 'Aggregation Induced Emission, AIE' that light emission is induced by aggregate formation,
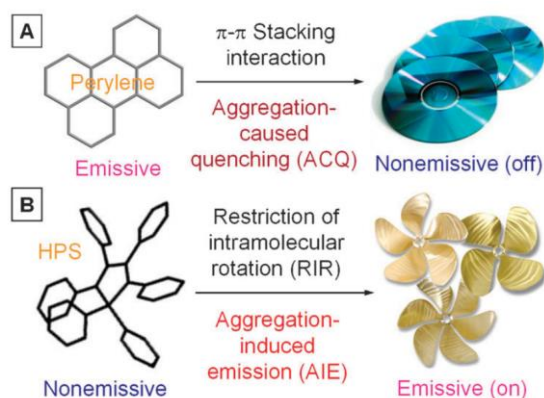
Figure 6. (a) Representative ACQ molecules, perylene derivatives, (b) The earliest reported AIE luminogen, Hexaphenylsilole (HPS).

Hexaphenylsilole (HPS) is among the first silole derivatives, from which the AIE phenomenon was unearthed. HPS can thus be considered a representative archetypal AIE luminogen. Structural investigation reveals that HPS is a propeller shaped non-planar molecule (Figure 6b). Tang explained that this difference in the molecular structure caused the novel emission behavior. In a dilute solution, six phenyl rotors in an HPS molecule undergo dynamic intramolecular rotations which dissipate non-radiatively its excited

6

state and results luminescent quenching. In the aggregates, however, the propeller shape of HPS inhibits the pi−pi interaction, restricting the intramolecular rotations of its aryl ring due to physical constraint. This phenomenon eliminate the non−radiative pathway caused by rotational relaxation and the luminescence intensity dramatically increases in aggregate form. Most conventional fluorescent chemosensors usually suffer from ACQ due to insolubility of organic fluorophores in water. Therefore, fluorescence sensors using AIE have been received significant attention in the last decade and provides a powerful solution for ACQ problem and offered a new strategy for designing fluorescent sensors.

1.2. Principle of Electrochemiluminescence (ECL)

Electrogenerated Chemiluminescence or Electrochemiluminescence (ECL) is a light emitting process through from electron transfer reaction between electrochemically generated radical species in a working electrode. For most of case, the emission spectrum is identical with ECL spectrum and same excited state would be formed in ECL. ECL is a powerful technic for analytical application. Due to absence of light source, it provides low background signal with high sensitivity and can be miniaturized to manufacture point-of-care test device.
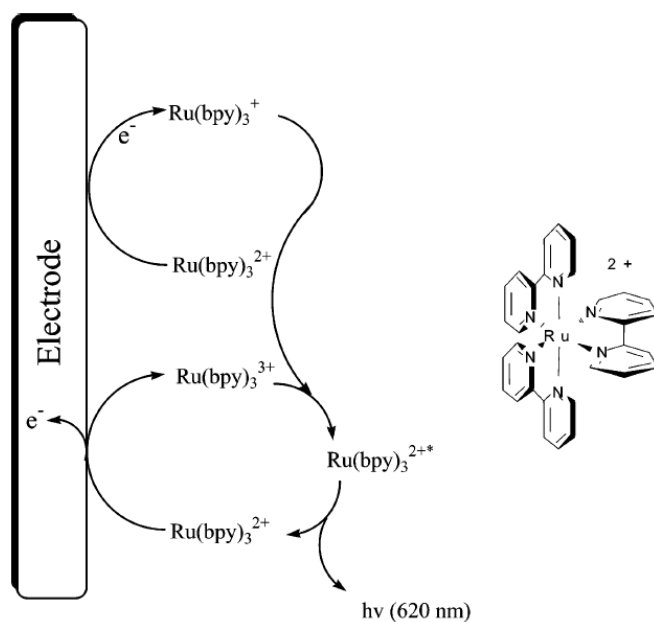
Figure 7. Schematic of annihilation ECL of $Ru(bpy_3)^{2+}$.

Annihilation ECL

Annihilation is the first reported method in ECL which involves electron transfer reactions between an oxidized and a reduced specie generated by alternating pulsing of electrode potential. then an excited molecule (e. g. $Ru(bpy)_3^{2+*}$) is produced around the electrode that emit light (Figure 7)[7]. General mechanism of annihilation ECL is presented below:

$$A - e^- \rightarrow A^{\bullet+} \text{ (oxidation at electrode)}$$
$$A + e^- \rightarrow A^{\bullet-} \text{ (reduction at electrode)}$$
$$A^{\bullet-} + A^{\bullet+} \rightarrow A^{\bullet} + A \text{ (excited-state formation)}$$
$$A^{\bullet} \rightarrow A + h\nu \text{ (light emission)}$$
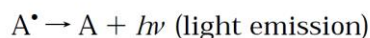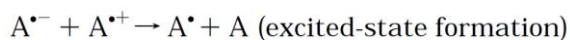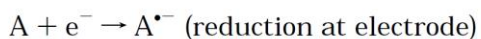
The luminophore produces a radical cation in anodic potential and a radical anion in cathodic potential. Then, these radical species react near the electrode surface to form the emissive state A^{*}. $Ru(bpy_3)^{2+}$ is one of the most efficient luminophores for ECL. Besides, organic compounds including Rubrene, Diphenyl Anthracene(DPA) and BODIPY are also well known compounds for annihilation ECL. (structures are presented below)
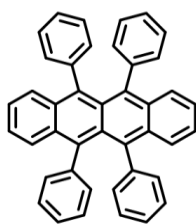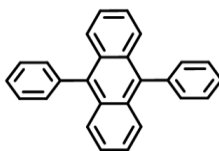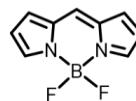
Rubrene   **DPA**   **BODIPY**

Co-reactant ECL

A method reported later but much more popularly used in ECL is "co-reactant ECL" that adds co-reactants to operate in single potential. A coreactant produces an intermediate upon oxidation or reduction that can react with an ECL luminophore (e. g. $Rubpy_3^{2+}$) to produce excited states ($Rubpy_3^{2+*}$). Most of commercially available analytical instruments using ECL are based on coreactant ECL method. This is because annihilation ECL is only applicable in organic solvent due to limited potential window of aqueous media. However, coreactant ECL provides stable electrochemical signals in aqueous solution which is essential for analysis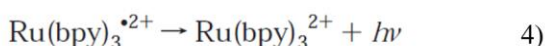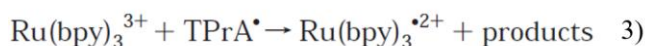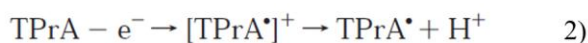 in biological environment. Many of coreactant ECL applications involve $Ru(bpy)_3^{2+}$ as a luminophore and Tri-n-propylamine (TPrA) as a coreactant. The mechanism for co-reactant ECL using TPrA is outlined below:

.

$$Ru(bpy)_3{}^{2+} - e^- \rightarrow Ru(bpy)_3{}^{3+} \qquad 1)$$

$$TPrA - e^- \rightarrow [TPrA^\bullet]^+ \rightarrow TPrA^\bullet + H^+ \qquad 2)$$

$$Ru(bpy)_3{}^{3+} + TPrA^\bullet \rightarrow Ru(bpy)_3{}^{\bullet 2+} + products \qquad 3)$$

$$Ru(bpy)_3{}^{\bullet 2+} \rightarrow Ru(bpy)_3{}^{2+} + h\nu \qquad 4)$$

Unlike annihilation ECL, both luminophore and coreactant are oxidized at the electrode in co-reactant ECL. The oxidized form of TPrA (TPrA radical cation) is very unstable and immediately lose a proton, forming the strongly reducing intermediate TPrA radical. Then, the oxidized luminophore, $Ru(bpy_3)^{3+}$ accept an electron from TPrA radical to produce excited state that emit light. Since reducing agents are formed upon electrochemical oxidation, coreactant ECL using TPrA is also called by "oxidative-reductive" pathway. Oxalate ($C_2O_4{}^{2-}$) is also known for oxidative-reductive coreactant, but the efficiency is usually much lower than TPrA system.

"Reductive−oxidative" ECL is also used for coreactant ECL. In this system, persulfate ($S_2O_8^{2-}$) are widely used coreactant. ECL luminophore, $Ru(bpy_3)^{2+}$ and these coreactant accept an electron from electrode and the latter generate strong oxidizing agent in cathodic potential. Then, reduced luminophore ($Rubpy_3^+$) oxidized to form the excited state ($Ru(bpy)_3^{2+*}$) emitting light. Benzoyl peroxide (BPO) is another coreactant that used in   reductive− oxidative ECL system. The ECL mechanism using persulfate is outlined below:

$$Ru(bpy)_3^{2+} + e^- \rightarrow Ru(bpy)_3^+ \qquad 5)$$

$$S_2O_8^{2-} + e^- \rightarrow SO_4^{\bullet-} + SO_4^{2-} \qquad 6)$$

$$Ru(bpy)_3^+ + SO_4^{\bullet-} \rightarrow Ru(bpy)_3^{\bullet 2+} + SO_4^{2-} \quad 7)$$
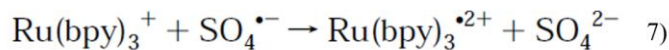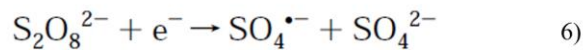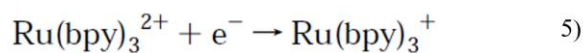
Cyclic voltammetry (CV) is a useful tool to investigate the electrochemical properties of co−reactants as well as luminophores. CV data also provides information about the stability of the oxidized and reduced forms of the complex and their ability to undergo electron transfer reactions.

1.3 Glutathione (GSH) Sensor
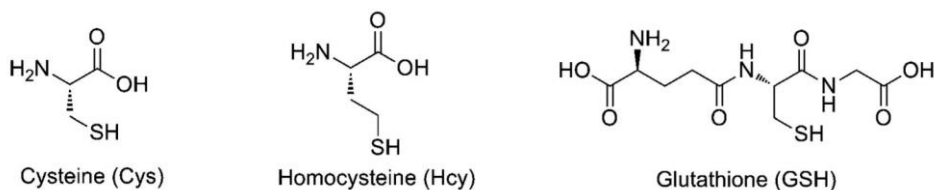
Figure 8. Structures of biological thiols.

Glutathione (GSH), a tripeptide composed of three amino acids (glutamic acid, cysteine and glycine), is one of the most important reducing agents in biological systems. GSH is involved in cellular processes, including cell differentiation, proliferation, and apoptosis. Decreased concentration of GSH leads to an increased susceptibility to oxidative stress implicated in cancer progression. Therefore, it is necessary to develop point-of-care testing (POCT) sensing systems measuring real-time concentration of GSH. However, it is challenging problem to selectively detect GSH from other structurally similar biological thiols, Cysteine (Cys) or Homocysteine (Hcy) due to their similar reactivity of same sulfhydryl group (-SH) (Figure 8).

Electrochemical detection, capillary electrophoresis, high performance liquid chromatography methods (HPLC) is well-known analytical methods for detecting GSH. However, these methods often require high cost and operational complexity, sample pretreatment and long analysis time. Thus, an alternative detecting method equipped with simple and inexpensive method is essential for GSH detection[8].

The development of fluorescent probes for GSH is the promising research area. Especially, a number of fluorescence probes utilizing unique reaction based on high nucleophilicity of sulfhydryl group of GSH have been reported. These include (a) Michael addition reactions[9] (b) cleavage of 2,4-Dinitro-benzosulfonamide(DNBS)[10], (c) cleavage of disulfide bond (S-S)[11],

(d) displacement of metal complex by thiols[12] (Figure 12). These thiol probes, however, have no selectivity in GSH due to similar reactivities as mentioned above.
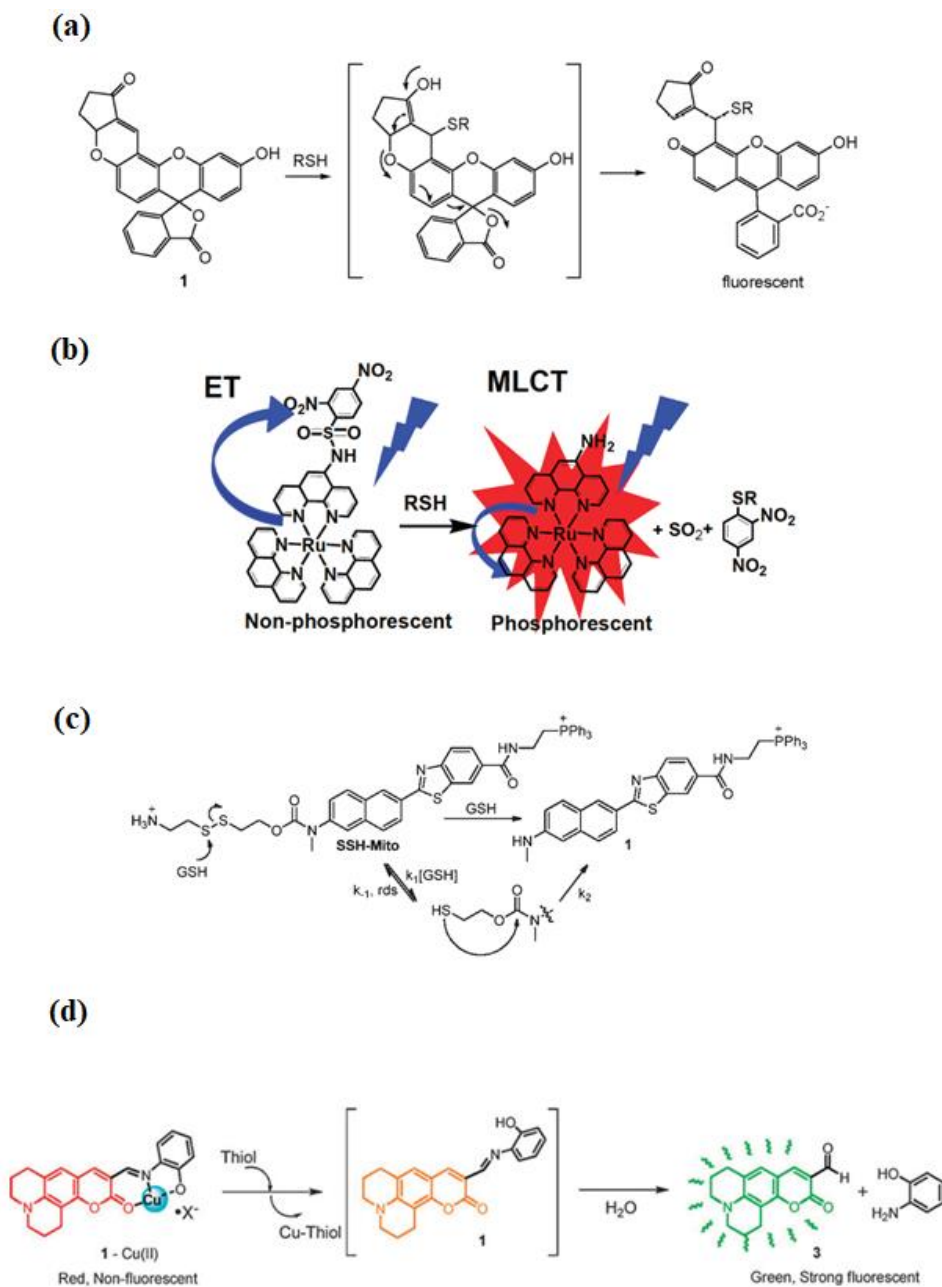

Figure 9. Fluorescent thiols probes using unique reaction between probe and thiols.

In order to detect GSH selectively, several researchers have reported novel reaction mechanism using structural difference of biological thiols.

The first thing is using 'smile rearrangement'. Q. Yang et al. synthesized mono-chlorinated BODIPY based GSH selective sensors in 2012[13]. These sensors have BODIPY core as fluorescent core and chloride (-Cl) that can be substituted by thiols (-SR)(Figure 13a). In the case of Cys and Hcy, the intramolecular primary amine further attacks the thiolate (which is called "smile rearrangement") and yield the amino-substituted BODIPY. However, GSH would require a kinetically unfavorable macrocyclic transition state to produce amino-substituted product. As a result, the sulfur-substituted BODIPY of GSH remains and shows distinct photophysical property that can be distinguished from other thiols.

The second thing is introduction of multi-recognition site. Wei Guo et al. reported unique fluorescent probe that detects Cys and GSH simultaneously from different emission channels[14]. This probe is consisted of chlorinated-hemicyanine luminophore with three potential reaction sites for biothiols. The first mechanism is same, which is S_NAr reaction of -SH group. Then, Cys and Hcy undergo smile rearrangement as above. Furthermore, the amino group of Cys attack the adjacent double bond (site 2) to form 7-membered ring. It is distinguished from Hcy due to kinetically unfavorable formation of 8-membered ring in case of Hcy. When reacting with GSH, neither the amino group undergo rearrangement nor attack the adjacent double bond. Instead, it could attack the other double bond (site 3) to form 14 membered ring. Consequently, Cys and GSH showed different emission channel and no emission from Hcy.
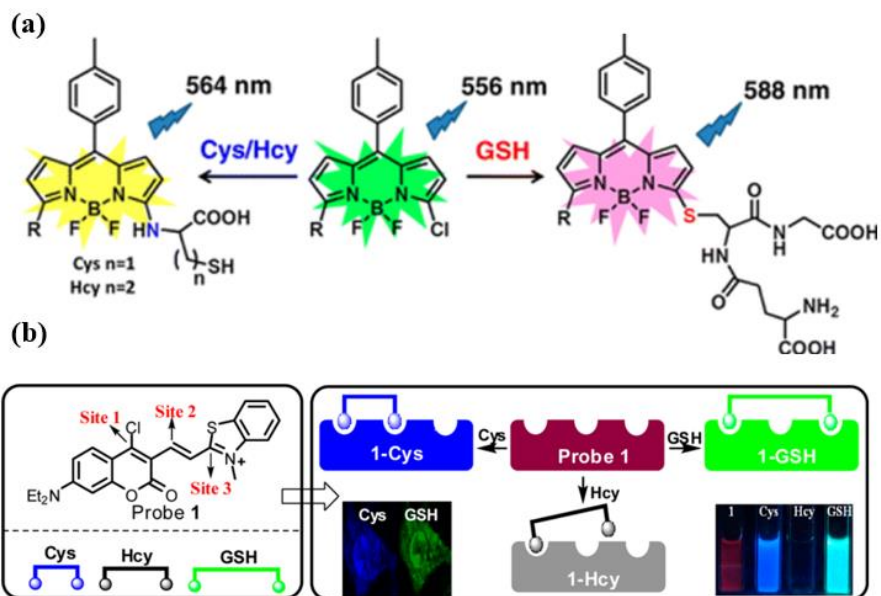
Figure 10. Fluorescent probes that can selectively detect GSH from other biological thiols with different emission channels.

1.4 Properties of Iridium(Ⅲ) Complexes and Application for ECL Sensor
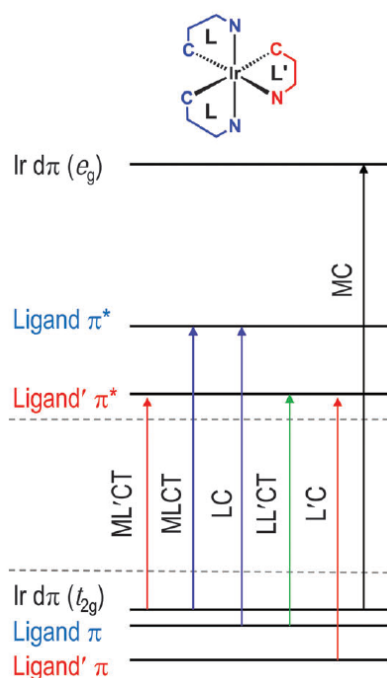
Figure 11. Schematics of the photophysical processes of typical hetero-leptic cyclometalated Ir(III) complexes.

Tris-cyclometalated Ir(III) complexes have a pseudo-octahedral coordination geometry, in which three mono-anionic bidentate ligands(N^C) occupy the six coordination sites of the Ir atom. Cyclometalated Ir(III) complexes are easily synthesized via a standard two-step procedure involving dimerization of the Ir(III) complex and following substitution with a third ligand to afford the octahedral Ir(III) complex[15].

The excited states of cyclometalated iridium complexes include metal-centered transition (MC), ligand-centered transition (LC), metal-to-ligand charge-transfer (MLCT), intraligand charge-transfer (ILCT) and so on (Figure 11). These states depend on the metal centers, excited state energy levels of the ligands, chemical structures, polarity of solvent and intermolecular interaction and so

on. It shows different emission wavelength, intensity and lifetime change if these conditions are changed. To design of phosphorescent chemosensor, It is need to understand and utilize the rich excited state properties of phosphorescent heavy-metal complexes [16].

Analytical application using co-reactant ECL has been predominantly based on the $Ru(bpy)_3^{2+}$ complexes because of its electrochemical stability, high ECL quantum yield and good water solubility with characteristic orange and red emissions. However, numerous iridium complexes have been investigated for the alternative ECL luminophore due to easy modification of electrochemical and photophysical property with little changes in the ligands. The Ir(III) complexes show excellent photoluminescence quantum yields (PLQY). These properties of iridium complexes have a possibility for development of multi-color or potential-resolved multiplexed ECL systems [17].

Several iridium complexes have been reported to deal with the fundamental understanding of low ECL intensity for the high PL intensity luminophore by selecting materials having a reduction potential lower than the coreactant, TPrA radical (Figure 12). It revealed that deeper HOMO and LUMO level (within marcus region) is important conditions for efficient electron transfer from TPrA radical to iridium complex, which resulting in strong ECL [18]. The iridium complexes having phenylquinoline (pq) main ligand showed much higher ECL intensity than those having phenylpyridine (ppy) main ligand due to lower LUMO energy levels despite the similar PLQY.
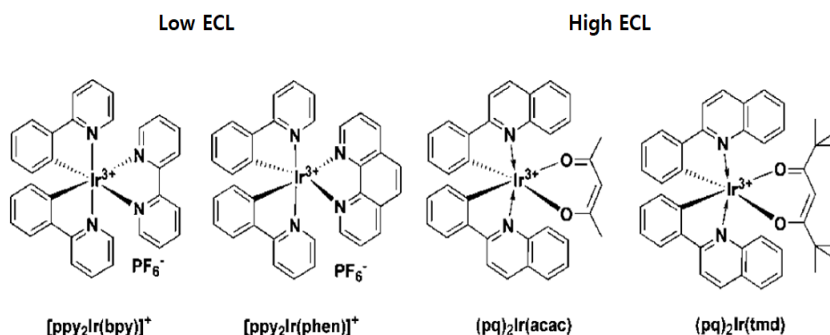
Figure 12. Iridium complexes that showed similar or higher ECL intensity than $Ru(bpy_3)^{2+}$.

Combining these iridium complexes and ECL technic with the design strategy of photoluminescent sensor, novel sensing platform for analytical method can be constructed by introducing the sensing mechanism (e. g. PeT, FRET, ESIPT, AIE, etc..) to ECL sensor. It is important for ECL luminophore to have electrochemical stability as well as high photoluminescence quantum yield in ECL sensor. Because electrochemically unstable luminophores should not provide a stable or enough signal in measurement of ECL.

Chapter 2. Iridium(Ⅲ) Complexes for Phosphorescent and Electrochemiluminescent Detection of GSH

2.1 Introduction

Glutathione(GSH) is one of the most important reducing agent in biological system which consists of glycine, cysteine, glutamate. The sulfhydryl group (–SH) of cysteine is involved in conjugation or reduction reactions that are critical roles of GSH[19, 20]. GSH is involved in cellular processes, including cell differentiation, proliferation, and apoptosis. Decreased concentration of GSH leads to an increased susceptibility to oxidative stress implicated in the progression of cancer[20, 21]. So it is necessary for developing point−of−care test (POCT) sensors measuring real−time concentration of GSH.

Photoluminescent sensor have favorable condition for analysis including non−invasiveness, high selectivity, sensitivity, low cost and operational simplicity. Accordingly, a number of photoluminescent sensors for detection of GSH have been reported. Most well−known strategies are using strong nucleophilicity of sulfhydryl (–SH) group of GSH for designing Michael−addition type sensors[22−25]. or S_NAr reaction−based sensors by introducing thiol−responsive leaving group[26−28]. Also multiple recognition site−based probes have been developed for selective detection of GSH among various structurally similar biological thiols[27−29]. Recently, several benzoquinone−based GSH sensors have been reported[30−35]. the quinone reacts with GSH by either Michael addition or electron transfer reaction.

Many fluorescent probes for detecting the cellular concentration of GSH have been reported. Even though structurally similar biological thiols such as cysteine (Cys) and homocysteine (Hcy) induce interfering signal to GSH sensors, the intracellular concentration of these molecules is much smaller than GSH[36−38]. In human blood serum, however, it is suggested that GSH (7−30 μM)

concentration is less than Cys (200−400 μM)[39, 40]. Therefore, considering that lots of POCT sensors measure GSH concentration from blood medium[41, 42], it is necessary to develop a sensor for selectively detecting GSH from Cys and Hcy in micromolar concentration.

Electrochemiluminescence (ECL) is a luminescent process induced by electron transfer reaction of radical species produced electrochemically at electrode surface. Unlike conventional photoluminescence, no light source for excitation is required for ECL, which is advantageous for low background signals and high sensitivity[7, 43]. Especially, coreactant ECL is efficient method to develop ECL sensor because it can be operated at narrow potential range necessary for aqueous solution and operable with small concentration of probes. For development of ECL luminophore, a variety of cyclometalated iridium(III) complexes have been reported due to its high luminescence quantum yield, electrochemical stability and easy modification[44−48].

Here, we synthesized heteroleptic cyclometalated iridium complex based GSH chemodosimeter, probe **1**, incorporating phenanthroline−dione (pdo) in auxiliary ligand as recognition site which can be detected by photoluminescence and electrochemiluminescence. We also synthesized probe **2** and **3** having different main ligands to compare the sensing efficiency. All these complexes have showed turn−on response for PL detection and turn−off response for ECL detection. We found that GSH reduce the dione group to diol group by using UV−VIS, NMR, FT−IR spectroscopy and Mass spectrometer. From the mechanistic study using density functional theory (DFT) and cyclic voltammetry, it was found that dione moiety provides non−radiative pathway for probes and eliminated in diol−moiety resulting turn−on PL response. In the case of ECL, diol group of reaction product (**1−GSH**) showed oxidation peak at anodic potential which indicates that oxidized radical of diol intercept the TPrA radical so that inhibit the efficient ECL process.

2.2   Result and discussion
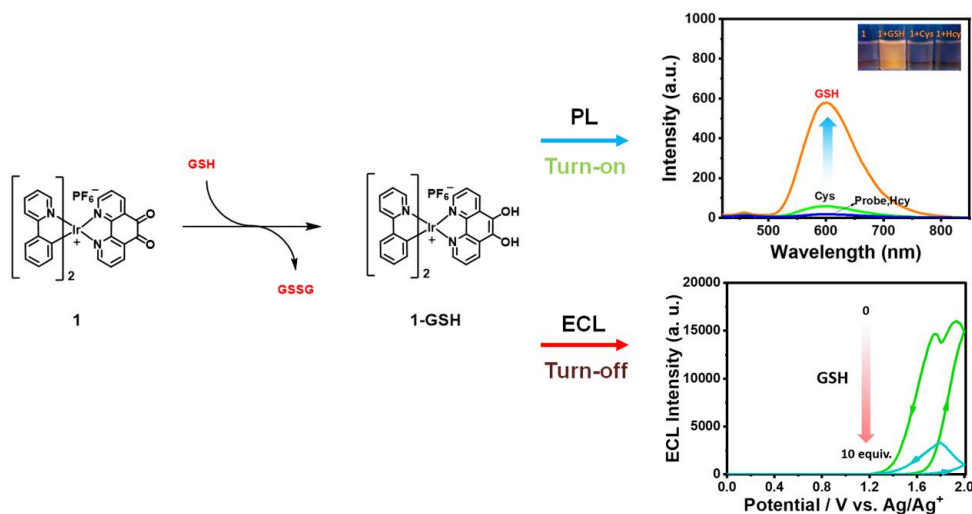
Figure 13. Design of Iridium complex−based GSH probe.

2.2.1 Design of probe

Glutathione is well known compound for its antioxidant capability. Recently, several groups have reported the benzoquinone−based probes for detection of GSH using Michael addition or electro−reduction. Especially, many fluorescent probes based on reduction mechanism have been reported using the superior reducing power of GSH.   Accordingly, we prepared iridium complex probe **1** having phenanthroline−dione (pdo) in ancillary ligand for GSH detection by PL and ECL method. Besides the probe **1** having phenylpyridine (ppy) as main−ligand, we synthesized additional iridium complexes **2** and **3** having phenylisoquinoline (piq) and phenylquinoline (pq) as main ligands respectively to compare the sensing efficiency.

2.2.2 Photophysical Properties of Iridium Complexes

First, we examined the photophysical properties of the synthesized iridium(III) complexes. We measured UV/Vis absorption (dashed line) and photoluminescence spectra (solid line) of Ir(III) complexes in a mixed solvent (CH_3CN/H_2O, 1:1 v/v, 10 mM HEPES, pH 7.4). All probes showed intense absorbances around 300 nm corresponding to ligand-centered transition (LC) and moderate absorption around 350 nm which is responsible for spin-allowed intraligand and metal to ligand charge transfer transition (^{1}ILCT, ^{1}MLCT). The broad absorption spectrum around 400~500 nm was attributed to spin forbidden intraligand and charge transfer transition state (^{3}ILCT, ^{3}MLCT). Probe **2** and **3** showed red-shifted absorption compared to probe **1** due to extended pi-conjugation structures. All the emission spectra were obtained when excited at 400 nm. The maximum emission intensity of probe **1** was achieved at 595 nm upon excitation giving a stokes shift of 195 nm. Probe **2** showed a similar but narrower emission spectrum than probe **1** and pronounced shoulder at 630 nm. Probe **3** showed maximum intensity at 560 nm which is 30 nm blue-shifted than probe **1** due to low lying HOMO energy[49].
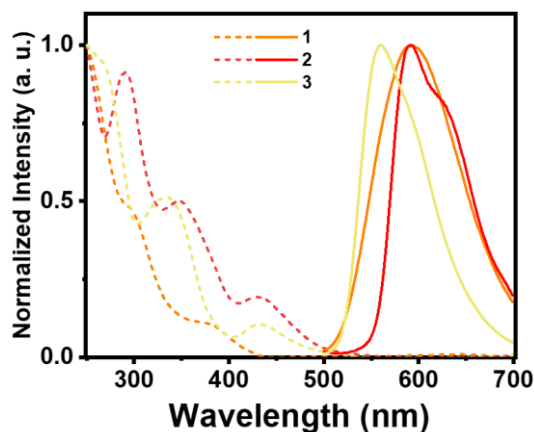
Figure 14. Photophysical properties of synthesized iridium complexes (10 μM). Condition: (CH_3CN/H_2O, 1:1 v/v, 10 mM HEPES, pH 7.4, excitation at 400 nm).

2.2.3 Photoluminescent Detection of GSH

Next, we investigated the photoluminescent response of probes toward biological thiols (Figure 15). First, we measured the absorption changes of probes when reacting with biological thiols (Figure 15a). While the absorbances around 300 nm were increased after the addition of thiols, there were no absorption changes around 400 nm which is excitation wavelength.

While, the emission intensity of all probes gradually increased and reached its plateau after the addition of 10 equivalents of GSH without remarkable wavelength changes when excited at 400 nm (Figure 15b). Especially, probe **1** showed 35 times increased PL intensity when saturated. Moreover, the interference signals produced by Cys and Hcy were quite negligible. probe **2** and **3** showed 10 times and 4 times turn-on response respectively (Figure 15c). Although probe **3** showed the most intense emission after reaction with GSH, the turn-on ratio was not that significant due to the relatively strong emission of probe itself. Linear calibration curves between PL intensity and added GSH concentration (0 ~ 40 μM) are presented (Figure 15c, Inset) and limit of detection (LOD) was calculated to 2.34 μM for **1**, 6.64 μM for **2**, and 3.31 μM for **3**.

We also conducted the selectivity test for other biological compounds and compared each maximum intensity of probes before and after the addition of analyte (Figure 15d). As expected, there were no remarkable luminescent changes by common amino acids including oxidized glutathione (GSSG) and even hydrogen sulfide (−SH) which is a strong nucleophilic biological thiol. However, vitamin C (Vc), one of the antioxidants, showed a notable interfering signal still not significant than GSH. This result suggests that the most plausible reaction mechanism between probes and GSH is electron-reduction rather than nucleophilic addition or substitution reaction. Probe **2** and **3** showed a similar tendency with probe **1** in the

selectivity test. However, the selectivity of both probes was greatly decreased.

Consequently, probe **1** showed the most selective and sensitive response to GSH from photoluminescent detection. All probes took several hours to achieve the maximum intensity after the addition of GSH (Figure 16). Encouragingly, all probes showed highest turn-on ratio at pH 7.4 which is favorable in biological system (Figure 17).
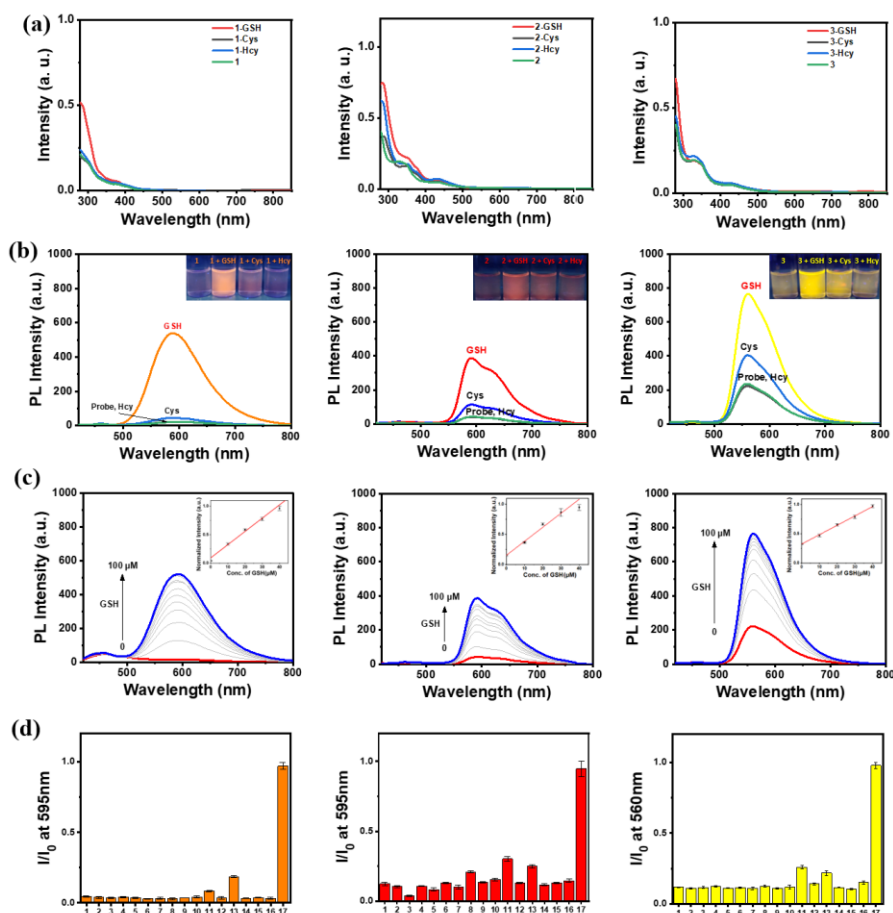
Figure 15. PL responses of sensors **1** (left), **2** (middle), **3** (right) in CH_3CN/H_2O (1:1, v/v, 10 mM HEPES, pH 7.4, 10 μM each sensor) (a) before and after the addition of biological thiols (Inset shows colorimetric changes of sensors under UV hand lamp), (b) in the presence of increasing concentrations (0 ~ 100 μM) of GSH, (c) with various amino acids, reducing agents, and oxidized form of GSH (100 μM each), (1) sensor only, (2) Thr, (3) Ser, (4) Met, (5) Ile, (6) His, (7) Asp, (8) Gly, (9) Pro (10) Hcy, (11) Cys, (12) NaHS, (13) Vc, (14) α-Tocopherol (15) D-Glucose (16) GSSG, (17) GSH.
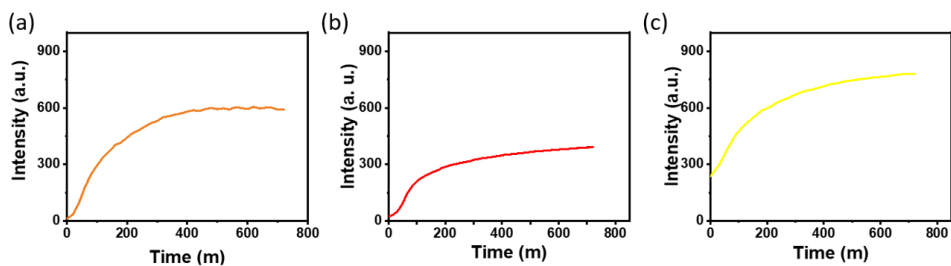
Figure 16. Time-dependent measurement of PL intensity changes of probe (a) **1**, (b) **2**, (c) **3** in a mixture of CH₃CN/H₂O (1:1, v/v, 10 mM HEPES, pH 7.4, 10 μM).
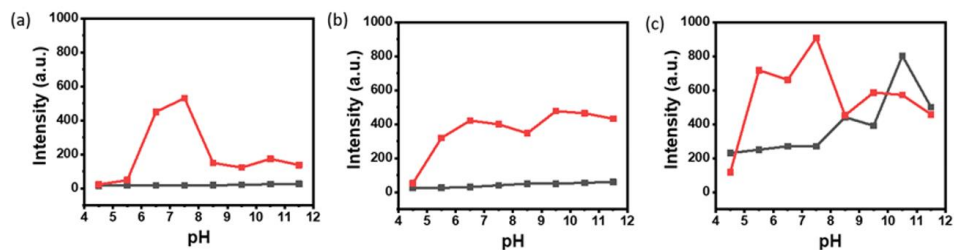
Figure 17. Comparison of photoluminescence intensity of probe (a) **1** (b) **2** (c) **3** under different pH condition before (gray line) and after (red line) the addition of GSH (10 eq.).
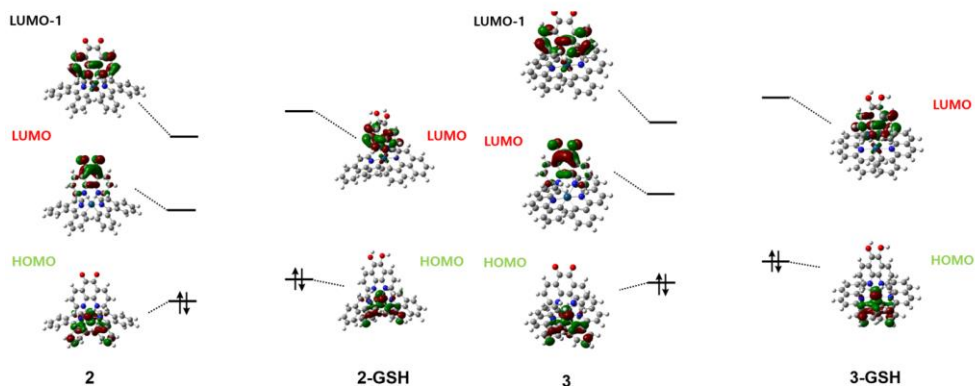
2.2.4 PL Turn-on mechanism study

To elucidate the turn-on response mechanism, probe **1** was chosen as a representative compound, and we synthesized the reaction product, **1-GSH**. The synthesized product was confirmed by NMR, FT-IR spectroscopy and Mass spectrometer (Figure 18). It was obvious that di-carbonyl group is reduced to di-hydroxyl group after reaction with GSH. Also, UV-Vis spectrum of **1-GSH** showed the same photoluminescent behavior with the mixture of probe **1** and GSH (Figure 18a). Next, we conducted a DFT calculation for probe **1** and **1-GSH**. The calculated orbital distribution and energy levels are presented in Figure 19. While LUMO of **1-GSH** is localized on bi-pyridyl moiety in pdo ligand, LUMO of probe **1** is localized on dione-moiety and its LUMO-1 have the same orbital distribution with LUMO of **1-GSH**. Considering that the optical band gap energy of probe **1** is about 2.74 eV (calculated from absorption onset), LUMO-1 to HOMO transition is responsible for the radiative pathway. Therefore, the weak PL of probe **1** is attributed to the non-radiative quenching by the dione moiety. In other words, the excited MLCT state which is localized on bi-pyridyl moiety rapidly relaxed to dione resulting in non-radiative decay according to energy gab law.

In fact, F. M. MacDonnell et al. suggested that semi-quinone [3]MLCT state is responsible for non-radiative decay pathway for [Ruphen$_2$pdo]$^{2+}$ complex[50] and D. E. Forbes et al. showed that dione-localized triplet state exists in [Rubpy$_2$pdo]$^{2+}$ complex which offers secondary energy transfer pathway for rapid relaxation of bi-pyridyl [3]MLCT state[51]. Both authors reported that hydration on these complex eliminates the quenching mechanism and restore photoluminescent capacity. In our case, As GSH reduces dione to diol, the quenching state is eliminated and restores its bright emission (Figure 19). We also obtained the same calculation results from probe **2** and **3** (Figure 20). These results were further evidenced by the control experiment using **1-Phen** having same

orbital distribution with **1-GSH** (Figure 21). As expected, **1-Phen** showed strong luminescence upon excitation.

Figure 18. Comparison of (a) UV-Vis spectrum (b) Mass spectrum (c) FT-IR spectrum (d) NMR spectrum of probe **1** and **1-GSH**.

Figure 19. Electron density distribution of frontier molecular orbitals and energy levels of probe **1** and **1-GSH** obtained by DFT calculation.

DFT Calculation: B3LYP/ LanL2DZ
(in vacuum condition)

Figure 20. Calculated orbital distribution of probe **2** and **3**.
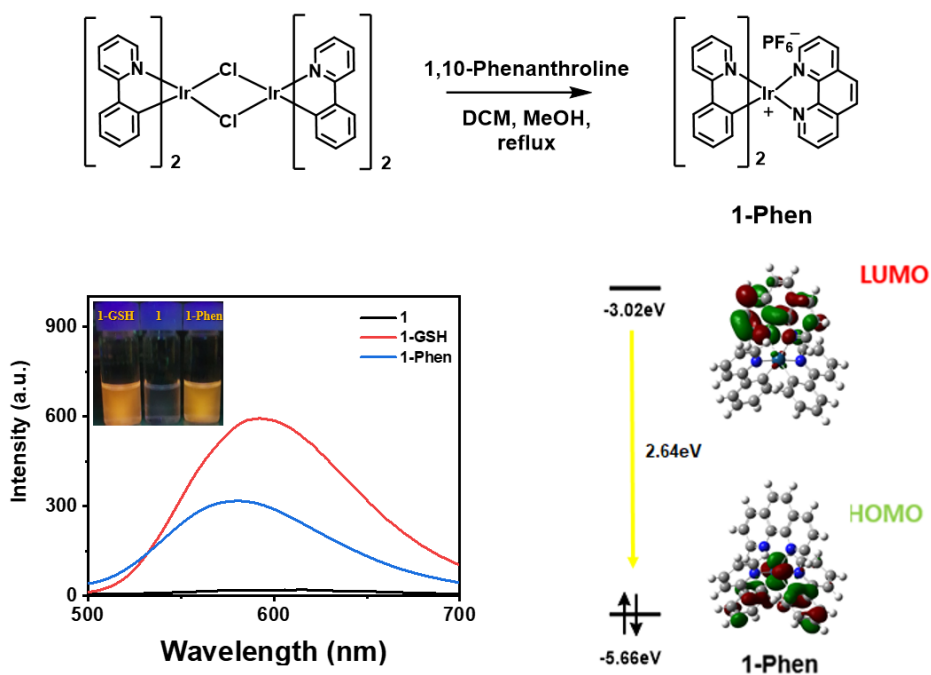

Figure 21. (Left) Comparison of emission spectrum of **1−Phen** complex with probe **1** and **1−GSH**. (Right) Calculated orbital distribution and energy levels of **1−Phen** complex.

## 2.2.5 Electrochemical Properties of Iridium Complexes

We investigated the electrochemical properties of iridium complexes using cyclic voltammetry in degassed acetonitrile solution. In anodic scan, iridium complexes showed quasi−reversible oxidation peaks derived from iridium center and phenyl ring without a remarkable difference in oxidation potential as well as electrochemical stability (Figure 22a). In a cathodic scan, two reversible one electron−reduction waves were observed at −0.4V and −1.0V from all probes. These peaks were assigned to the reduction of dione by comparing with the cyclic voltammogram of free phenanthroline−dione (pdo) and phenanthroline−diol (phen(OH)$_2$) (Figure 22b). it is well known that pdo is an electroactive compound and the di−carbonyl group is reduced to the di−hydroxyl group. The reduction potentials of pdo in iridium complexes are shifted positive relative to those of the free pdo ligand due to the coordination to the metal center[52, 53]. It showed further negative reduction potentials in all probes which are attributed to the reduction of main ligand(C^N) and bi−pyridyl ligand(N^N). It showed almost same reduction potentials around −1.9V despite the difference of main ligands. This is because the second−lowest occupied molecular orbitals (LUMO−1) of all probes are localized in the same bi−pyridyl moiety (Figure 19, 20).
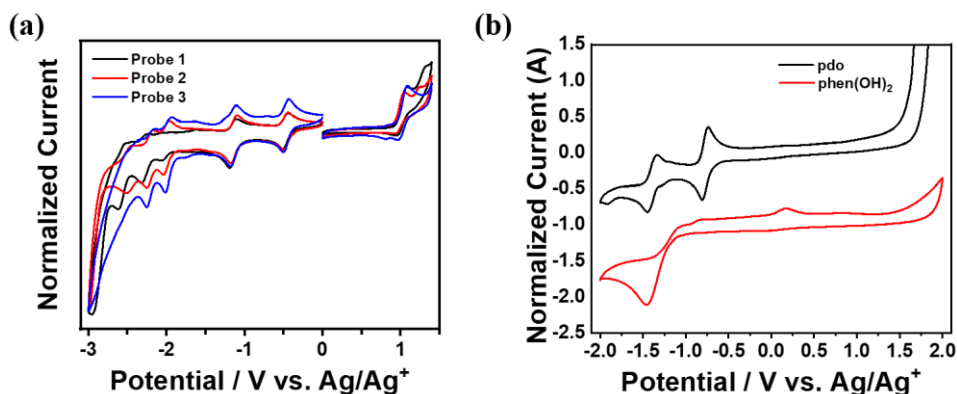
Figure 22. Cyclic voltammograms of (a) probe **1**, **2**, **3** and (b) free pdo and phen(OH)$_2$ ligand measured in degassed acetonitrile with 0.1 M TBAP as supporting electrolyte, scan rate 0.1 V/s.

2.2.6 Electrochemiluminescent detection of GSH

Finally, we investigated the ECL response for probe **1** with the addition of GSH in a mixed aqueous solution (Figure 23). Interestingly, the results showed opposite results to the PL experiment. While significant strong ECL was observed in probe **1**, it was dramatically decreased with the addition of GSH (Figure 23a). The ECL intensity of probe **1** decreased exponentially and saturated with 3 equivalents of GSH (Figure 23b). The ECL intensity against negative logarithm concentration of GSH showed a linear calibration curve and the correlation coefficient $R^2=0.99$ was achieved. The LOD was calculated to 0.701 μM with a signal to ratio, S/N=3.
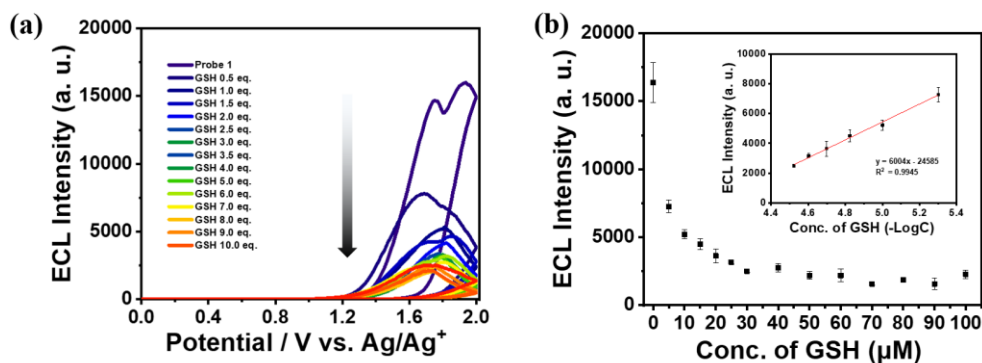
Figure 23. (a) ECL intensities of probe **1** (10 μM) after addition of GSH (0~100 μM) and other thiols (100 μM) in CH_3CN/H_2O (1:1 v/v, pH 7.4, 100 mM TPrA, 100 mM HEPES, and 0.1 M TBAP as a supporting electrolyte). (b) The potential was swept in the range 1.0－2.0 V (scan rate 0.1 V/s).

We then conducted the competitive ECL test for GSH with various biological compounds (Figure 24). The addition of common amino acids, structurally similar thiols (Cys, Hcy, NaHS) did not induce a remarkable ECL intensity changes. With the following addition of GSH, however, dramatically decreased ECL was observed. So probe **1** could detect GSH selectively from other biological compounds with high selectivity using ECL.
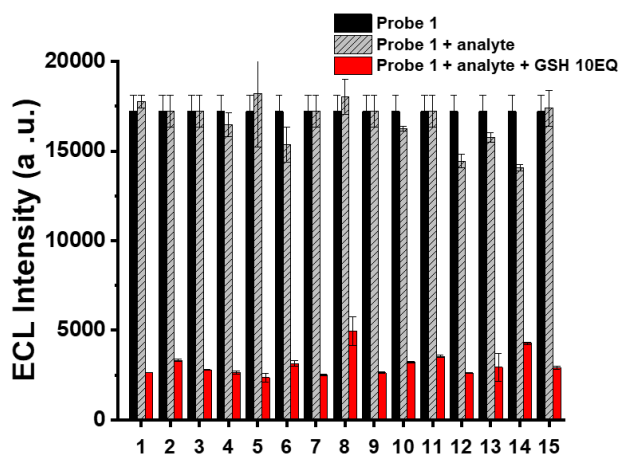
Figure 24. ECL intensity of probe **1** before (black bar) and after addition of each analyte (100 μM) in the absence (gray bar) and presence (red bar) of GSH. (1) Thr, (2) Ser, (3) Met, (4) Ile, (5) His, (6) Asp, (7) Gly, (8) Pro (9) Hcy, (10) Cys, (11) NaHS, (12) D−Glucose, (13) Tocopherol, (14) Vc, (15) GSSG.

Next, we tested the ECL response of other synthesized iridium complexes. It was found that probe **2** and **3** showed lower ECL than probe **1** (Figure 25). After the addition of GSH, each probes showed a turn−off response as probe **1**. However, the sensitivities were much lower compared to probe **1** due to the decreased ECL intensity and turn−off ratio (Figure 26).
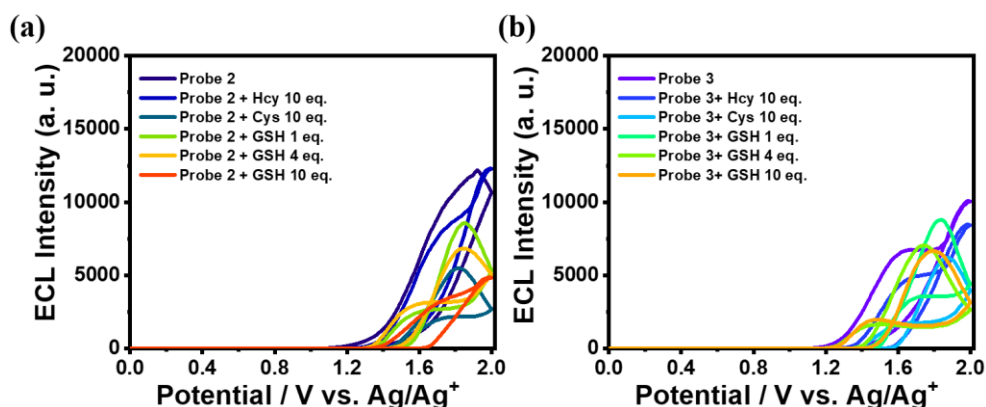
Figure 25. ECL intensities of probe **2** and **3** (10 μM) after addition of GSH (0, 40,100 μM) and other thiols (100 μM) in CH_3CN/H_2O (1:1 v/v, pH 7.4, 100 mM TPrA, 100 mM HEPES, and 0.1 M TBAP as the supporting electrolyte) while the potential is swept in the range 1.0−2.0 V (scan rate 0.1 V/s).
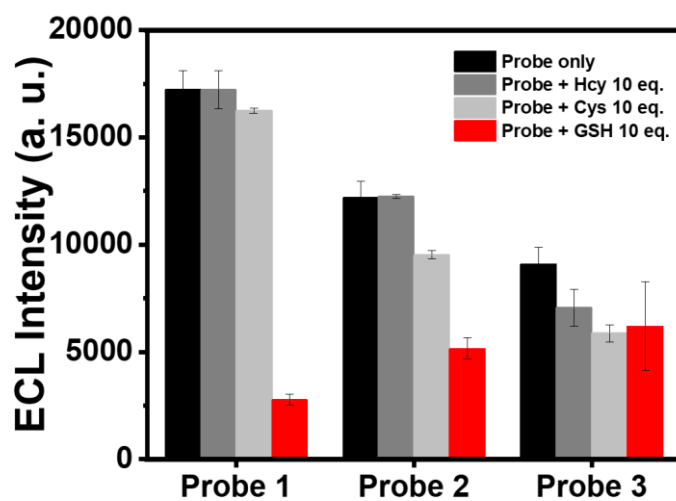
Figure 26. Comparison of ECL intensity of all probes before and after addition of biological thiols.

2.2.7 ECL Turn-off Mechanism Study

As mentioned above, contrary to PL experiments, sensor **1** exhibited decreased ECL with the addition of GSH. In fact, the ECL efficiency is not necessarily dependent on the PL quantum yield[54-58]. It was suggested that LUMO energy levels are good predictors of the co-reactant ECL efficiency[55]. If the LUMO level is raised over TPrA radical level (SOMO), the electron transfer process would be highly suppressed, which consequently inhibits the ECL process. However, it was found that the LUMO energy level (calculated from differential pulse voltammetry (DPV)) of **1-GSH** increased just 0.1 eV higher than probe **1** which is still lower than TPrA radical level. Therefore, this explanation is not enough to support ECL turn-off mechanism (Figure 27).
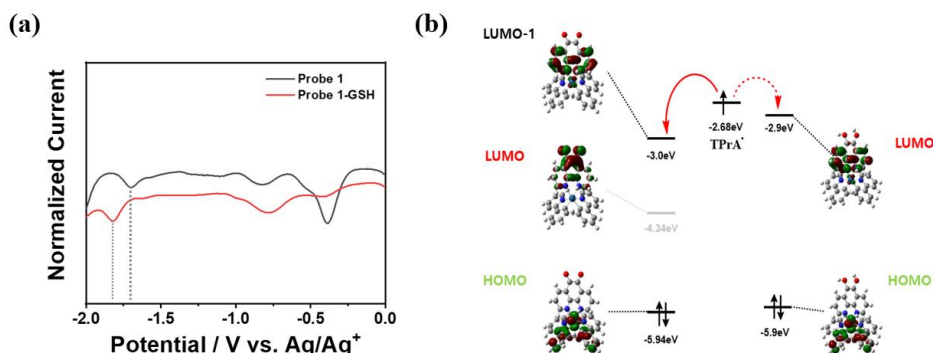
Figure 27. (a) DPV of probe **1** and **1-GSH** measured in CH_3CN (0.1M TBAP as supporting electrolyte) (b) Comparison of LUMO energy levels of **1** and **1-GSH** that calculated from DPV with TPrA radical SOMO energy level.

Meanwhile, phenol or catechol derivatives are well-known compounds for their ECL quenching capability[59, 60]. In the ECL process, there is two predominant pathway accounting for quenching mechanism of these compounds. The first thing is an excited-state quenching of luminophore by oxidized product of phenolic compound. The second thing is a radical interception reaction of phenolic radical with TPrA radical. The first mechanism was reasonably excluded considering the strong ECL of probe **1**. Therefore, in order to examine the effect of ligand oxidation, we first investigated the electrochemical behavior of phenanthroline-diol using cyclic voltammetry (Figure 22b). This ligand showed an irreversible oxidation peak at 0.146V which is attributed to the oxidation of hydroxyl group. Next, we measured the cyclic voltammetry of **1** after addition of GSH under CH$_3$CN/H$_2$O (v/v 4.5:1, 10 mM HEPES, pH 7.4, 0.1M TBAP) and compared it with the solution containing only GSH (Figure 28a). The mixture of **1** and GSH showed two oxidation peaks attributed to the oxidation of the hydroxyl group that were not observable in probe **1** (Figure 28b). Thus, we concluded that the produced phenolic radical in anodic potential interrupts the ECL process of **1-GSH** resulting in decreased ECL. (Figure 28c).
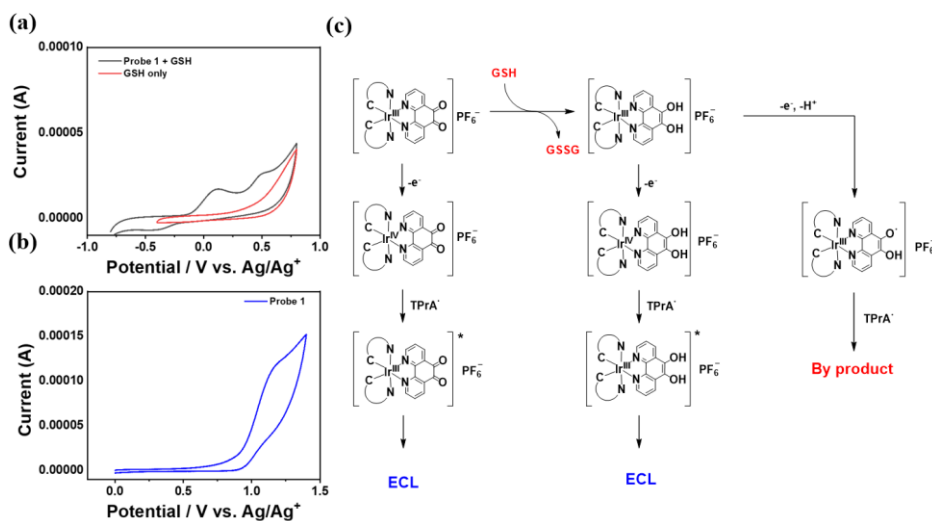

Figure 28. Cyclic voltammograms and presented ECL mechanism of probe **1** and **1-GSH**.

3 4

2.2.8 Potential clinical application

Quantitative analysis of GSH in a real sample was performed using probe **1,** which showed the best performance for GSH detection in both PL and ECL experiments

To apply the standard addition method to this ECL system in human serum, an additional linear calibration curve for probe **1** was obtained in the range of 0 to 5 μM of GSH (Figure 29). However, standard addition curve for probe **1** under the diluted serum was obtained in the range of 0 to 3 μM of GSH (Figure 30). The results are summarized in Table 1, demonstrating a good recovery of GSH concentration from 88.1 to 103.9%. The relative standard deviation (RSD) is in the range of 1.43 to 3.00%. After applying the dilution factors to the samples, we found that the original concentration of GSH in human serum was 19.16 μM. These values are within the range of the previously reported value of GSH in normal human blood serum (7~30 μM)[39, 40]. Therefore, compound **1** would be a potential candidate for POCT ECL sensors that can measure GSH concentrations in human serum.
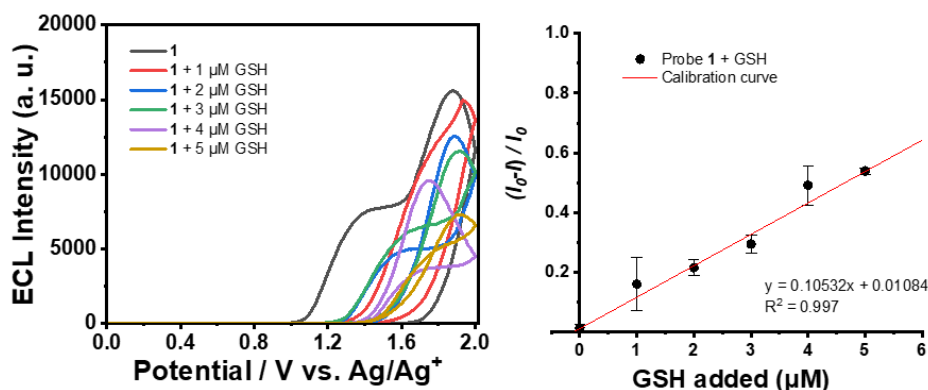
Figure 29. (a) ECL intensity changes of **1** after addition of GSH (0 to 5 μM) and (b) linear calibration curve in the mixture of CH_3CN/H_2O (1:1 v/v, pH 7.4, 10 mM HEPES, 100 mM TPrA and 0.1 M TBAP as a supporting electrolyte).

Table 1. Determination of GSH concentrations in human serum by ECL

Added GSH (μM)	Found (μM)[a]	Recovery (%)	RSD (n=3, %)[c]
–	0.479[b]	–	–
0	0.523	–	3.00
1	1.36	88.1	1.96
2	2.55	103.9	1.46
3	3.44	98.6	1.82

[a]The serum samples were diluted 40−fold with a 1:1 (v/v) mixture of HEPES buffer solution (10 mM, pH 7.4) and acetonitrile (0.1 M TBAP as supporting electrolyte). [b]The original concentration of GSH in diluted serum was determined by extrapolating the calibration curve at the point of y = 0.0203 which corresponds to the ECL intensity of **1** after the addition of N−ethylmaleimide (NEM, used for GSH masking agent) to the diluted serum (Figure 30b). [c]All data were obtained as the average of three separate measurements.
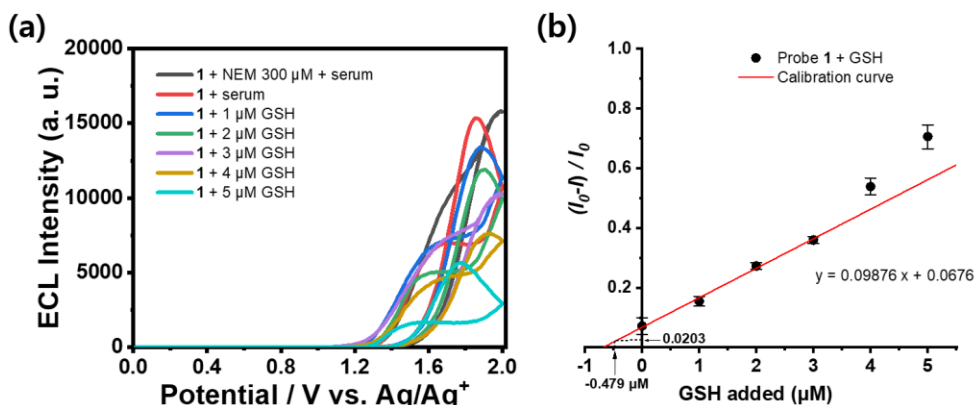
Figure 30. (a) ECL intensity changes and (b) standard addition curve of **1** after addition of GSH (0 to 3 μM) in 40−fold diluted serum.

2.3　Conclusion

We synthesized three cyclometalated iridium complexes having pdo ancillary ligand which can selectively react with GSH among not only other reducing agents but also structurally similar thiols (Hcy, Cys) in the micromolar concentration range. All sensors showed PL turn-on responses and ECL turn-off response for GSH. Sensor **1** having the phenylpyridine main ligand showed the most selective and sensitive response in both PL and ECL. DFT calculation revealed that the 1,2-dicarbonyl moiety of the ancillary ligand provides a non-radiative quenching pathway, resulting in fluorescence quenching, while radiative pathway is recovered upon reduction of the 1,2-dione moiety to diol by GSH. On the contrary, the electrochemical study demonstrated that interception of TPA radicals by phenolic radical species from **1-GSH** disturbs the ECL process, leading to decrease in the ECL intensity upon addition of GSH. Furthermore, **1** was successfully applied to quantitative measurements of GSH in human serum with a good reliability. We expect that compound **1** could be a promising candidate for point-of-care testing of GSH as a biomarker for human disease.

2.4   Experimental Details

2.4.1 Materials and Instruments

All reagents were purchased from either Sigma-Aldrich (Sigma-Aldrich Corp., MO, USA), TCI (Tokyo Chemical Industry, Tokyo, Japan), or Alfa Aesar (USA). used without any further purification. Deuterated solvents were acquired from CIL (Cambridge Isotopic Laboratories, MA, USA). Merck silica gel 60 F254 on aluminum foil was used for analytical thin layer chromatography. SiliaFlash® P60 (230–400 mesh) from SILICYCLE was used as the stationary phase in chromatographic separation. ^{1}H and ^{13}C NMR spectra were measured by Agilent 400-MR DD2 Magnetic Resonance System (USA), and Varian 500 MHz NMR System (USA). Chemical shifts (δ) were reported in ppm (chloroform=$CDCl_3$, dimethyl sulfoxide=DMSO-d_6). Absorption spectra were measured by using Beckman Coulter DU 800 Series spectrophotometer. Fluorescence emission spectra were measured by JASCO FP-6500 spectrometer with band width 5 nm. Matrix-assisted laser desorption/ionization time-of-flight (MALDI-TOF) mass measurements were performed using a Microflex (Bruker Daltonics). FT-IR spectra were acquired using spectrometer (PerkinElmer, Spectrum Two) and each samples were measured in diluted DCM solution. High-resolution mass spectrometry (JEOL, JMS-700) data were obtained with fast atom bombardment (FAB) positive mode from the National Center for Inter-University Research Facilities (NCIRF)

## 2.4.2 Electrochemical and Electrochemiluminescent Experiments

All Electrochemical experiments were conducted with a CH Instruments 650B Electrochemical Analyzer (CH Instruments, Inc., TX, USA). Cyclic voltammetry (CV) and Differential pulse voltammetry (DPV) technics were carried out on each solution to investigate electrochemical behavior. Three electrode system in electrochemical cell was used for CV and DPV measurement. Glassy carbon (GC) electrode was used for working electrode and Platinum (Pt) wire for counter electrode. All potential values were calibrated against the saturated calomel electrode (SCE) by measuring the oxidation potential of 1 mM ferrocene (vs. Ag/Ag^+) as the standard $(E_o(Fc/Fc^+) = 0.474V$ vs. SCE). All ECL experiments were performed using Pt disc working electrode (3 mm diameter) and Ag wire quasi-reference electrode at a scan rate of 0.1 V/s. All ECL spectra were acquired using a low-voltage Photomultiplier tube (PMT) module operated at 1.0 V. (H-6780 series, Hamamatsu photonics K. K., Tokyo, Japan). 250 µL ECL cell was directly mounted on the PMT module with a custom-made mounting support during experiments. Before every measurement, the working electrode was polished with 0.05 M alumina (Buehler, IL, USA) on a felt pad and sonicated with 1:1 mixture of distilled water and absolute ethanol for 5 min. Then the electrode was treated with ultra-high pure nitrogen (N_2) for 30 seconds. 0.1 M tetrabutylammonium perchlorate (TBAP, 98.0% TCI for ECL, and 99.0% analytical grade, Sigma-Aldrich for CV) used as supporting electrolyte and acetonitrile (99.9 % for spectroscopy, Across) for solvent. tri-n-propylamine (TPrA, Sigma-Aldrich, MO, USA) was used for co-reactant and diluted to 100 mM. ECL values were obtained by averaging the values from at least three data sets with good reliability in mixed solution of acetonitrile and water (1:1, v/v, 10 mM HEPES, pH 7.4). All of stock solution for photophysical and electrochemical experiments have been prepared by dissolving

compounds in DMSO to make 2 mM solution and stored in refrigerator and used freshly in every measurement. All of analyte solution (amino acids and reducing agents) have been prepared by dissolving compounds in 10 mM HEPES (pH 7.4) at 2 mM right before experiments. All of solution were not recycled.

Human serum samples (from human male AB plasma, USA origin, sterile-filtered, Aldrich) were stored at −80℃ in small aliquots. The serum was deproteinized by centrifugation at 6000 rpm for 10 min after precipitation with acetonitrile. The supernatant obtained after removal of acetonitrile was diluted 40-fold with a 1:1 (v/v) mixture of HEPES buffer solution (10 mM, pH 7.4) and acetonitrile (0.1 M TBAP as supporting electrolyte) before analysis.

2.4.3 Synthesis

Synthesis of Auxiliary Ligand (Pdo)
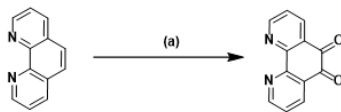
Synthetic Scheme of probe 1, 2, 3
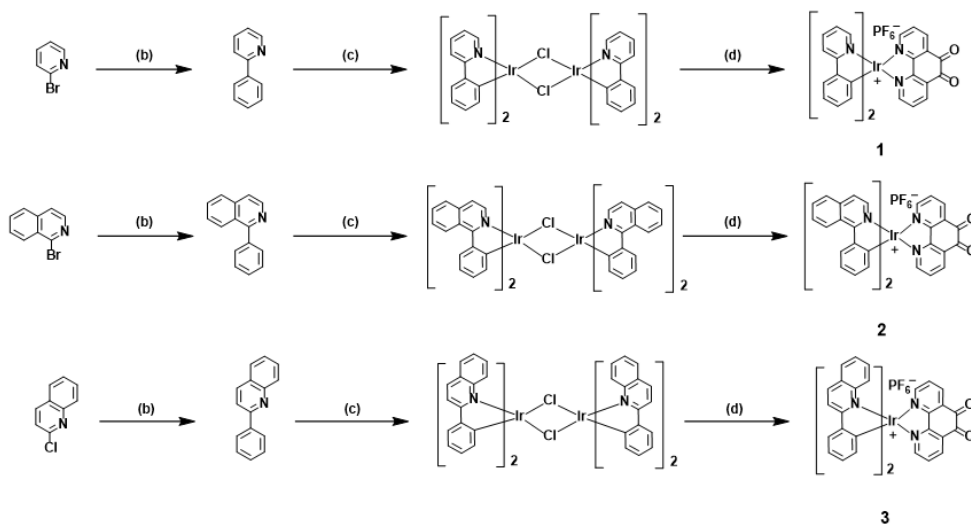
Figure 31. Synthetic scheme of the ligands and iridium complexes Condition: (a) H_2SO_4, HNO_3, KBr, 0°C → 90° (b) Phenylboronic acid, $Pd(PPh_3)_4$, K_2CO_3, THF, H_2O, reflux; (c) $IrCl_3 \cdot xH_2O$, 2-ethoxyethanol, H_2O, reflux; (d) 1,10-phenanthroline-5,6-dione, DCM, MeOH, reflux/ NH_4PF_6, DCM, MeOH, r. t.

Synthesis of 1,10-Phenanthroline-5,6-dione (Pdo)

The synthesis of 1,10-phenanthroline-5,6-dione was reported elsewhere[61]. To a 40 mL of an ice-cold concentrated H_2SO_4 was added a mixture of 2.0 g of 1,10-phenanthroline (11.1 mmol) and 4.0 g of KBr (33.6 mmol) with small portion. After the mixture was stirred for 20 min, 10 mL of concentrated HNO_3 was slowly added at room temperature and the mixture solution was refluxed at 90 ℃ for 3 h. The mixture was then cooled, poured on 200 mL ice and then carefully adjusted to pH 5~6 using NaOH. Then the aqueous

4 1

solution was extracted with CH_2Cl_2. The collected green−yellow extract was dried over Na_2SO_4 and the solvent removed in vacuo. After recrystallization from CH_2Cl_2 and Ether, bright yellow solid was obtained (1.45g, 62% yield). ^{1}H NMR (499 MHz, $CDCl_3$) δ 9.11 (dd, J = 4.6, 1.8 Hz, 2H), 8.49 (dd, J = 7.9, 1.8 Hz, 2H), 7.58 (dd, J = 7.8, 4.7 Hz, 2H).

Synthesis of 2−Phenylpyridine (ppy)

A mixture of 2−bromopyridine (1.26 g, 8.0 mmol), phenylboronic acid (1.07 g, 8.8 mmol), K_2CO_3 (3.3g, 24.0 mmol) and $Pd(PPh_3)_4$ (277 mg, 0.24 mmol) in THF (80 mL) and H_2O (80 mL) was refluxed for 7 h. Then the solution was allowed to cool to room temperature. The organic layer was washed with water and extracted with dichloromethane (30 mL X 3) then dried over Na_2SO_4 and concentrated in vacuo. The product was purified using flash chromatography on silica gel with hexane and CH_2Cl_2 (1:1 v/v) and concentrated in vacuo to afford yellowish−white liquid. (0.664 g, 4.28 mmol, 54%). ^{1}H NMR (400 MHz, $CDCl_3$) δ 8.79 – 8.61 (m, 1H), 8.03 – 7.92 (m, 2H), 7.73 (ddd, J = 4.4, 2.8, 1.5 Hz, 2H), 7.53 – 7.43 (m, 2H), 7.41 (dd, J = 5.0, 3.6 Hz, 1H), 7.25 – 7.21 (m, 1H).

Synthesis of [Irppy₂(μ−cl)]₂

A mixture of 2−phenylpyridine (664 mg, 4.3 mmol) and iridium tri−chloride hydrate (512 mg, 1.7 mmol) in 2−ethoxyethanol (45 mL) and H_2O (15 mL) was refluxed for 20 hours. The solution was cooled to room temperature and stirred with the addition of 50 mL water. Then the precipitate was filtered and thoroughly washed with water and ethanol. The resulting pale−green solid was dried in IR lamp over 12 hours and used for next step without further purification. (290 mg, 0.27 mmol, 32%), ^{1}H NMR (499 MHz, $CDCl_3$) δ 9.23 (d, J = 5.2 Hz, 4H), 7.86 (d, J = 7.9 Hz, 4H), 7.73 (t, J = 7.0 Hz, 4H), 7.47 (d, J = 7.7 Hz, 4H), 6.79 – 6.70 (m, 8H), 6.55 (t, J = 7.5 Hz, 4H), 5.92 (d, J = 7.7 Hz, 4H).

Synthesis of 1

Probe **1** was prepared according to reported method with a little revision[32]. [Irppy$_2$(μ-cl)]$_2$ (0.08 g, 0.074 mmol) and 1,10-phenanthroline-5,6-dione (29 mg, 0.13 mmol) in a mixture of dichloromethane and methanol (2:1, 15 mL) was refluxed overnight under a N$_2$ atmosphere. The solution was evaporated in vacuo and purified with flash chromatography with DCM/MeOH (10:1). The resulting product was dissolved in dichloromethane and methanol (1:1, 10 mL) again and stirred for 4 hours with the addition of ammonium hexafluorophosphate (NH$_4$PF$_6$) (20 mg, 0.1 mmol). After evaporation, the organic layer was washed with water and extracted with dichloromethane (10mL X 3). then concentrated in vacuo, and recrystallized from DCM and Ether to afford brown solid. (40 mg, 31% yield). ^{1}H NMR (400 MHz, DMSO-d$_6$) δ 8.65 (d, J = 7.5 Hz, 2H), 8.27 (d, J = 8.4 Hz, 2H), 7.99 (s, 2H), 7.93 (dd, J = 12.7, 8.0 Hz, 4H), 7.86 (s, 2H), 7.59 (d, J = 5.5 Hz, 2H), 7.17 (t, J = 6.7 Hz, 2H), 7.02 (t, J = 7.5 Hz, 2H), 6.90 (t, J = 7.4 Hz, 2H), 6.17 (d, J = 7.4 Hz, 2H). ^{13}C NMR (500 MHz, DMSO-d$_6$) δ 174.38, 167.19, 155.21, 153.14, 149.62, 149.49, 144.22, 139.49, 137.10, 132.43, 131.50, 130.80, 130.19, 125.63, 124.27, 123.02, 120.62. HRMS (FAB) calcd for C$_{34}$H$_{23}$IrN$_4$O$_2$ [M+H]$^+$ 712.1450, found 712.1466.

Synthesis of 2 and 3

Probe **2** and **3** were prepared according to same procedure with probe **1** except that 2-phenylisoquinoline (piq) or 2-phenylquinoline (pq) were used instead of 2-phenylpyridine (ppy).

Probe **2**, (32 mg, 0.0335 mmol, 37%). ^{1}H NMR (400 MHz, DMSO-d$_6$) δ 8.98 (d, J = 9.3 Hz, 2H), 8.66 (s, 1H), 8.35 (d, J = 8.1 Hz, 2H), 8.18 – 8.02 (m, 2H), 8.02 – 7.83 (m, 7H), 7.63 (d, J = 6.6 Hz, 3H), 7.48 (d, J = 6.3 Hz, 2H), 7.12 (t, J = 7.8 Hz, 2H), 6.91 (t, J = 7.6 Hz, 2H), 6.17 (d, J = 7.3 Hz, 2H). ^{13}C NMR (500 MHz,

dmso-d$_6$) δ 174.37, 168.24, 155.04, 153.09, 152.85, 145.56, 141.11, 137.12, 137.10, 137.06, 132.66, 132.52, 131.90, 131.17, 131.08, 130.16, 129.92, 128.13, 126.91, 125.98, 122.99, 122.52. HRMS (FAB): m/z observed for C$_{42}$H$_{27}$IrN$_4$O$_2$$^+$ [M+H]$^+$ 812.1819, calculated for 812.1763

Probe **3**, (80 mg, 0.084 mmol, 49%). ^{1}H NMR (400 MHz, DMSO-d$_6$) δ 8.63 – 8.45 (m, 6H), 8.28 (dd, J = 14.7, 6.5 Hz, 4H), 7.97 – 7.78 (m, 4H), 7.41 (d, J = 6.2 Hz, 2H), 7.20 – 7.01 (m, 6H), 6.80 (t, J = 7.5 Hz, 2H), 6.36 (d, J = 7.5 Hz, 2H). ^{13}C NMR (500 MHz, DMSO-d6) δ. 174.54, 170.74, 151.05, 148.13, 147.10, 141.76, 138.08, 135.15, 132.63, 131.74, 130.44, 129.31, 128.96, 128.75, 128.11, 125.79, 124.23, 119.37. HRMS (FAB): m/z observed for C$_{42}$H$_{27}$IrN$_4$O$_2$$^+$ [M+H]$^+$ 812.1838 calculated for 812.1763

Reference

1. B. Valeur, *Digital Encyclopedia of Applied Physics*, 2003, 477-531.
2. Z. Liu, W. He and Z. Guo, *Chem. Soc. Rev.*, 2013, **42**, 1568-1600.
3. X. Lou, D. Ou, Q. Li and Z. Li, *Chem Commun (Camb)*, 2012, **48**, 8462-8477.
4. L. Yuan, W. Lin, K. Zheng and S. Zhu, *Acc. Chem. Res.*, 2013, **46**, 1462-1473.
5. A. C. Sedgwick, L. Wu, H.-H. Han, S. D. Bull, X.-P. He, T. D. James, J. L. Sessler, B. Z. Tang, H. Tian and J. Yoon, *Chem. Soc. Rev.*, 2018, **47**, 8842-8880.
6. Y. Hong, J. W. Lam and B. Z. Tang, *Chem. Soc. Rev.*, 2011, **40**, 5361-5388.
7. M. M. Richter, *Chem. Rev.*, 2004, **104**, 3003-3036.
8. H. S. Jung, X. Chen, J. S. Kim and J. Yoon, *Chem. Soc. Rev.*, 2013, **42**, 6019-6031.
9. Z. Liu, X. Zhou, Y. Miao, Y. Hu, N. Kwon, X. Wu and J. Yoon, *Angew. Chem.*, 2017, **129**, 5906-5910.
10. S. Ji, H. Guo, X. Yuan, X. Li, H. Ding, P. Gao, C. Zhao, W. Wu, W. Wu and J. Zhao, *Org. Lett.*, 2010, **12**, 2876-2879.
11. C. S. Lim, G. Masanta, H. J. Kim, J. H. Han, H. M. Kim and B. R. Cho, *J. Am. Chem. Soc.*, 2011, **133**, 11132-11135.
12. H. S. Jung, J. H. Han, Y. Habata, C. Kang and J. S. Kim, *Chem. Commun.*, 2011, **47**, 5142-5144.
13. L.-Y. Niu, Y.-S. Guan, Y.-Z. Chen, L.-Z. Wu, C.-H. Tung and Q.-Z. Yang, *J. Am. Chem. Soc.*, 2012, **134**, 18928-18931.
14. J. Liu, Y.-Q. Sun, Y. Huo, H. Zhang, L. Wang, P. Zhang, D. Song, Y. Shi and W. Guo, *J. Am. Chem. Soc.*, 2014, **136**, 574-577.
15. Y. You and W. Nam, *Chem. Soc. Rev.*, 2012, **41**, 7061-7084.
16. Q. Zhao, F. Li and C. Huang, *Chem. Soc. Rev.*, 2010, **39**, 3007-3030.
17. G. J. Barbante, E. H. Doeven, E. Kerr, T. U. Connell, P. S. Donnelly, J. M. White, T. Lópes, S. Laird, D. J. D. Wilson, P. J. Barnard, C. F. Hogan and P. S. Francis, *Chem. Eur. J.*, 2014, **20**, 3322-3332.
18. J. I. Kim, I.-S. Shin, H. Kim and J.-K. Lee, *J. Am. Chem. Soc.*, 2005, **127**, 1614-1615.
19. H. J. Forman, H. Zhang and A. Rinna, *Mol Aspects Med*, 2009, **30**, 1-12.
20. S. Agrawal, B. Winnik, B. Buckley, L. Mi, F.-L. Chung and T. J. Cook, *J. Chromatogr. B*, 2006, **840**, 99-107.
21. N. Traverso, R. Ricciarelli, M. Nitti, B. Marengo, A. L. Furfaro, M. A. Pronzato, U. M. Marinari and C. Domenicotti, *Oxid. Med. Cell. Longev.*, 2013, **2013**, 972913.
22. M. Tian, M. Yang, Y. Liu and F.-L. Jiang, *ACS Appl. Bio Mater.*, 2019, **2**, 4503-4514.
23. Z. Liu, X. Zhou, Y. Miao, Y. Hu, N. Kwon, X. Wu and J. Yoon, *Angew. Chem. Int. Ed. Engl.*, 2017, **56**, 5812-5816.

24. X. Jiang, J. Chen, A. Bajić, C. Zhang, X. Song, S. L. Carroll, Z.-L. Cai, M. Tang, M. Xue, N. Cheng, C. P. Schaaf, F. Li, K. R. MacKenzie, A. C. M. Ferreon, F. Xia, M. C. Wang, M. Maletić-Savatić and J. Wang, *Nat. Commun.*, 2017, **8**, 16087.

25. X. Jiang, Y. Yu, J. Chen, M. Zhao, H. Chen, X. Song, A. J. Matzuk, S. L. Carroll, X. Tan, A. Sizovs, N. Cheng, M. C. Wang and J. Wang, *ACS Chem. Biol.*, 2015, **10**, 864-874.

26. J. Chen, Z. Wang, M. She, M. Liu, Z. Zhao, X. Chen, P. Liu, S. Zhang and J. Li, *ACS Appl. Mater. Interfaces*, 2019, **11**, 32605-32612.

27. F. Chen, D. Han, H. Liu, S. Wang, K.-B. Li, S. Zhang and W. Shi, *Analyst*, 2018, **143**, 440-448.

28. C.-X. Yin, K.-M. Xiong, F.-J. Huo, J. C. Salamanca and R. M. Strongin, *Angew. Chem. Int. Ed.*, 2017, **56**, 13188-13198.

29. G.-x. Yin, T.-t. Niu, Y.-b. Gan, T. Yu, P. Yin, H.-m. Chen, Y.-y. Zhang, H.-t. Li and S.-z. Yao, *Angew. Chem. Int. Ed.*, 2018, **57**, 4991-4994.

30. Q. Han, F. Zhou, Y. Wang, H. Feng, Q. Meng, Z. Zhang and R. Zhang, *Molecules*, 2019, **24**, 2455.

31. Y. Xu, L. Zhang, Y. Liu, Z. Jin, Q. Zhao, F. Yang and D. Xiao, *Biosens. Bioelectron.*, 2016, **77**, 182-187.

32. Z. Mao, J. Liu, T.-S. Kang, W. Wang, Q.-B. Han, C.-M. Wang, C.-H. Leung and D.-L. Ma, *Sci Technol Adv Mater*, 2016, **17**, 109-114.

33. H.-W. Liu, X. Zhu, J. Zhang, X.-B. Zhang and W. Tan, *Analyst*, 2016, **141**, 5893-5899.

34. X. Dai, Z.-F. Du, L.-H. Wang, J.-Y. Miao and B.-X. Zhao, *Anal. Chim. Acta*, 2016, **922**, 64-70.

35. F. Yu, P. Li, P. Song, B. Wang, J. Zhao and K. Han, *Chem. Commun.*, 2012, **48**, 4980-4982.

36. C. Wang, X. Xia, J. Luo and Y. Qian, *Dyes Pigm.*, 2018, **152**, 85-92.

37. J. Zhang, B. Yu, L. Ning, X. Zhu, J. Wang, Z. Chen, X. Liu, X. Yao, X. Zhang and H. Zhang, *Eur. J. Org. Chem.*, 2015, **2015**, 1711-1718.

38. J. Lu, Y. Song, W. Shi, X. Li and H. Ma, *Sens. Actuators B Chem.*, 2012, **161**, 615-620.

39. D. Ścibior, M. Skrzycki, M. Podsiad and H. Czeczot, *Clin. Biochem.*, 2008, **41**, 852-858.

40. Q. Hu, C. Yu, X. Xia, F. Zeng and S. Wu, *Biosens. Bioelectron.*, 2016, **81**, 341-348.

41. C. P. Chan, W. C. Mak, K. Y. Cheung, K. K. Sin, C. M. Yu, T. H. Rainer and R. Renneberg, *Annu Rev Anal Chem (Palo Alto Calif)*, 2013, **6**, 191-211.

42. Y. Song, Y.-Y. Huang, X. Liu, X. Zhang, M. Ferrari and L. Qin, *Trends Biotechnol.*, 2014, **32**, 132-139.

43. Z. Liu, W. Qi and G. Xu, *Chem. Soc. Rev.*, 2015, **44**, 3117-3142.

44. L. Chen, E. H. Doeven, D. J. Wilson, E. Kerr, D. J. Hayne, C. F. Hogan, W. Yang, T. T. Pham and P. S. Francis, *ChemElectroChem*, 2017, **4**, 1797-1808.

45. J. M. Fernandez-Hernandez, E. Longhi, R. Cysewski, F. Polo, H.-P. Josel and L. De Cola, *Anal. Chem.*, 2016, **88**, 4174-4178.

46. Y. Zhou, H. Gao, X. Wang and H. Qi, *Inorg. Chem.*, 2015, **54**, 1446–1453.

47. K. N. Swanick, S. Ladouceur, E. Zysman-Colman and Z. Ding, *Angew. Chem.*, 2012, **124**, 11241–11244.

48. W. Miao, *Chem. Rev.*, 2008, **108**, 2506–2553.

49. C. D. Sunesh, R. K. Chitumalla, M. S. Subeesh, K. Shanmugasundaram, J. Jang and Y. Choe, *J. Electroanal. Chem.*, 2016, **780**, 249–256.

50. S. A. Poteet, M. B. Majewski, Z. S. Breitbach, C. A. Griffith, S. Singh, D. W. Armstrong, M. O. Wolf and F. M. MacDonnell, *J. Am. Chem. Soc.*, 2013, **135**, 2419–2422.

51. R. D. Schmidt, C. A. Kent, J. J. Concepcion, W. Lin, T. J. Meyer and M. D. E. Forbes, *Dalton Trans.*, 2014, **43**, 17729–17739.

52. C. A. Goss and H. D. Abruna, *Inorg. Chem.*, 1985, **24**, 4263–4267.

53. D. M. Murphy, K. McNamara, P. Richardson, V. Sanchez-Romaguera, R. E. P. Winpenny and L. J. Yellowlees, *Inorg. Chim. Acta*, 2011, **374**, 435–441.

54. J. I. Kim, I.-S. Shin, H. Kim and J.-K. Lee, *J. Am. Chem. Soc.*, 2005, **127**, 1614–1615.

55. G. J. Barbante, E. H. Doeven, E. Kerr, T. U. Connell, P. S. Donnelly, J. M. White, T. Lópes, S. Laird, D. J. D. Wilson, P. J. Barnard, C. F. Hogan and P. S. Francis, *Chem. Eur. J.*, 2014, **20**, 3322–3332.

56. H. Rhee, T. Kim and J.-I. Hong, *Dalton Trans.*, 2018, **47**, 3803–3810.

57. J. Park, T. Kim, H. J. Kim and J.-I. Hong, *Dalton Trans.*, 2019, **48**, 4565–4573.

58. H. J. Kim, T. Kim and J.-I. Hong, *Sens. Actuators B Chem.*, 2020, **307**, 127656.

59. J. McCall, C. Alexander and M. M. Richter, *Anal. Chem.*, 1999, **71**, 2523–2527.

60. H. Zheng and Y. Zu, *J. Phys. Chem. B*, 2005, **109**, 16047–16051.

61. U. Udeochu, T. Jimerson, A. Vivoni, O. Bakare and C. M. Hosten, *J. Phys. Chem. A*, 2007, **111**, 3409–3415.

국문초록

글루타티온(GSH)은 인간의 몸 속에 가장 풍부하게 존재하는 생물학적 티올이며, 생체 환원제로 작용한다. GSH의 결핍은 암의 진행을 초래하는 산화적 스트레스와 관련이 있다. 따라서 GSH을 선택적으로 검출할 수 있는 방법이 요구되고 있다.

본 연구에서는 GSH을 선택적으로 검출하기 위한 이리듐 콤플렉스 기반의 광 발광(PL) 및 전기화학발광(ECL) 센서를 보고한다. 센서 1-3는 공통적으로 GSH을 인식할 수 있는 페난트롤린 다이온 (pdo) 보조 리간드가 있으며, 각각 페닐 피리딘, 페닐 이소퀴놀린, 페닐 퀴놀린을 주 리간드로 갖는다. 이를 통하여, 주 리간드의 차이가 GSH 검출에 대한 선택성과 민감도에 갖는 영향을 비교하였다. 센서가 GSH와 반응하고 난 뒤 PL 신호를 관찰하였을 때, 모든 센서의 신호는 증가하는 감응을 보인 반면, ECL을 이용한 검출에서는 모든 센서의 신호가 감소하는 감응을 보였다. 특히, 페닐 피리딘 주 리간드를 가진 센서 1은 PL과 ECL 실험 모두에서 가장 높은 선택성과 민감도를 보여주었다. 센서 1의 di-carbonyl 부분은 GSH와 반응 시에 di-hydroxyl (1-GSH)로 환원되었고 이는 핵자기 공명법, 적외선 분광법, 질량 분석법으로 증명하였다.

우리는 PL과 ECL에서 나타나는 검출 메커니즘을 각각 규명하기 위해 센서 1에 대하여 분자 오비탈의 분포와 전기화학적 특성을 조사하였다. 밀도 범함수 이론 계산 결과, 센서 1의 di-carbonyl 부분에 LUMO가 분포하여 비발광 경로를 제공하였다. 하지만, GSH와 반응 시에 이러한 메커니즘이 사라지면서 PL 신호가 크게 증가하였다. 반면에, 센서 1와 GSH의 혼합물을 순환 전압전류법으로 조사해본 결과, 산화 전위를 인가할 때 phenolic radical이 생성되는 것을 알 수 있었다. 따라서, phenolic radical이 1-GSH의 ECL 과정을 억제하기 때문에 센서 1이 GSH와 반응한 후에는 ECL 신호가 크게 감소하였다.

마지막으로, 센서 1을 이용하여 사람의 혈청 (blood serum) 내 GSH을 성공적으로 검출함으로써, 센서 1을 이용하여 현장 진단용 GSH 검출 장비를 만들 수 있는 가능성을 보였다.

주요어: 글루타티온 (GSH), 이리듐 콤플렉스, 단분자 센서, 광 발광, 전기화학발광, 순환 전압전류법.

학번: 2019-26006

감사의 글

2년 동안 이곳에서 연구뿐만 아니라 여러 선배님들과 생활하는데 있어서 많은 것을 배우고 성숙해지는 과정을 겪었습니다. 졸업 후, 박사 과정을 시작하게 되면 더 많은 것을 배우고 도전해야 하기에 전보다 겸손하고 다른 사람을 배려하는 마음으로 임하도록 하겠습니다.

먼저, 항상 저를 믿어주시고 가장 사랑해주시는 가족들에게 감사의 말을 전합니다. 특히, 엄마는 항상 새로운 기회를 만들어주시고 포기하지 말라고 이끌어주시는, 세상에서 저에게 가장 귀한 은인입니다. 그리고 대학원의 길을 선택하는데 도움을 주고 대학원 생활 중에도 많은 조언을 해준 누나에게도 감사의 말을 전합니다.

그리고 연구뿐만 아니라, 영적으로나 일상생활에서 저에게 조언과 격언을 아끼지 않으셨던 저의 지도교수 홍종인 교수님에게 감사의 말을 전합니다. 얼마 남지 않은 기간 동안 박사과정에 임하도록 허락해 주시고 저를 신뢰해 주셔서 감사드립니다. 그에 보답하도록 열심히 임하겠습니다. 또, 제 학위논문을 심사하고 수고해주시는 민달희 교수님, 이현우 교수님께도 감사의 말을 전합니다.

마지막으로, 실험실 선배님들과 저의 사수이자 인생의 선배로써 저에게 항상 힘이 되어주신 태민이 형에게 감사의 말을 전합니다. 제가 실험도 못하고 남들과 잘 어울리지 못해도 항상 저의 고민과 어려운 일을 상담해주시고 늘 남들에게 겸손하고 좋은 관계를 유지하라던 당부를 잊지 않도록 하겠습니다. 감사합니다.

2021년 2월

노현승 드림